**Fachhochschule Dortmund**
**University of Applied Sciences and Arts**
**Embedded Systems Engineering**

# A Comparative Analysis of System Architectures for Collaborative SLAM

## Research Thesis

Fachhochschule Dortmund
University of Applied Sciences and Arts

**Author:** Aditya Kumar
**Matriculation Number:** 7219675
**Supervisor:** Prof. Dr. Stefan Henkler
**Co-Supervisor:** You Co-Supervisor(s)
**Date:** February 5, 2026

# Abstract

Collaborative Simultaneous Localisation and Mapping (C-SLAM) enables teams of robots to construct a shared environment map while estimating their trajectories. As multi-robot systems move toward larger deployments in dynamic settings, the backend architecture becomes a primary determinant of end-to-end performance. However, experimentally controlled comparisons between different C-SLAM architectures with similar frontend-backend processing under realistic network effects remain scarce.

This research thesis presents a systematic, implementation-grounded comparison of two representative backend paradigms within a unified evaluation framework. A centralised incremental pose-graph optimiser and a decentralised DDF-style distributed optimiser. To ensure architectural fairness, both backends consume identical pre-computed factor streams from the COSMO-Bench dataset and are evaluated using a fully automated ROS 2 testbed that can apply packet loss, transmission delay, and bandwidth limitations in a controlled manner. Performance is quantified using localisation accuracy, latency and convergence behaviour, communication bandwidth, and computational resource utilisation.

The centralised backend provides more dependable global consistency and convergence across the investigated setups, especially as team size grows. However, it results in significantly higher uplink communication and concentrates processing at the server. Although the decentralised backend achieves quick local update responsiveness and much reduced communication requirements, it is more sensitive to impaired peer-to-peer information transmission and coordination overhead at scale.

Overall, neither centralised nor decentralised C-SLAM paradigms are universally optimal. Their effectiveness depends on specific application needs. Centralised C-SLAM is preferable when infrastructure is stable, precision and global consistency are important, robots have limited hardware, and team sizes are small to medium. Decentralised C-SLAM, on the other hand, is appropriate for inconsistent connectivity, critical scalability, strict fault tolerance, and situations requiring more autonomy.

# Declaration

I, Aditya Kumar, hereby confirm, that I have written the Research Thesis at hand independently – in case of a group work: my respectively designated part of the work -, that I have not used any sources or materials other than those stated, and that I have highlighted any citations properly. .
Dortmund, February 5, 2026

Aditya Kumar

# Contents

# List of Figures

# List of Tables

# 1

# Introduction

## 1 Motivation

In recent years, a sharp increase in the use of autonomous systems in a multitude of domains has driven significant advances in the field of robotics. These systems have been used in various industries, such as healthcare [27], transportation [26], and manufacturing [15], to improve efficiency, precision, and overall performance.

In this increasingly interconnected and complex world, the limitations of single-agent, centralised, monolithic systems are becoming more apparent. As a result, there is a growing trend towards the development of multi-agent systems that can work collaboratively and adaptively to tackle complex problems. These systems are able to distribute decision-making and problem-solving processes across multiple agents, allowing greater flexibility, scalability, and efficiency in the face of dynamic environments. A multi-agent system is selected as a solution to problems that are naturally more distributed, large, and complex for a single agent to solve. Implementation of these systems in problem domains such as search and rescue operations [9], environmental monitoring [13], precision agriculture [23] where these systems can be used to monitor crop health and control pest infestations, and mapping of archaeological sites [20].

While multi-agent systems are distributed in their true nature, the design and architecture for coordination and communication between multiple agents must be carefully planned to ensure seamless collaboration and task completion. This involves developing algorithms that enable agents to share information,

make decisions collectively, and adapt to changing environments in real time. A fundamental requirement for these coordinated tasks is a shared, real-time understanding of the environment, often represented as a global map. This is especially critical in scenarios where external positioning systems like GPS are inconsistent or unavailable entirely, necessitating a self-contained perception solution. For a traditional single-agent system this is solved by Simultaneous Localisation and Mapping *(SLAM)* [29], which allows the agent to build a map of its environment while simultaneously localising itself within that map. In a multi-agent setting this is extended to collaborative SLAM. *C-SLAM* leverages multiple robots working together to overcome the limitations of single-agent systems, such as limited perspectives, error accumulation over time, and challenges of large-scale complex environments. By sharing sensory information and coordinating efforts, multi-agent teams can create more accurate and robust maps while also increasing operational efficiency [35].

## 2 Problem statement

While many factors contribute to successful development and deployment of a C-SLAM system, architecture plays a vital role. Architectural choices determine-how sensing, communication, and optimisation workloads are distributed across robots and infrastructure, and directly affect scalability, robustness, and real-time performance. Key architectural paradigms, ranging from *purely centralised* setup where all map building and optimisation tasks are offloaded on a centralised server to *decentralised* where each robot maintains a local estimate and global consistency is recovered through distributed coordination. Each paradigm introduces inherent trade-offs in estimation accuracy, communication bandwidth requirements, computational load, and tolerance to network impairments.

Architectural selection in C-SLAM systems often relies on intuition, with decentralized architectures recognized for their robustness and scalability due to eliminating single points of failure. However, they may incur higher latency from increased coordination needs. In contrast, centralized pipelines offer faster global consistency but can become bottlenecks as team sizes grow or network conditions worsen. Despite these widely held assumptions and a substantial existing research on C-SLAM architectures and optimisation techniques, most studies evaluate systems under idealised or loosely controlled communication conditions, or focus on a single architectural paradigm in isolation. As a result, there is a lack of systematic, controlled and reproducible comparative assessment that isolates architectural effects, characterises latency and convergence under increasing collaboration scale, and relates performance to computational and communication constraints. Addressing this gap is necessary to enable principled architectural selection rather than assumption-driven design.

# 3 Research goals

The primary objective of this research project is to conduct and establish an evidence-based understanding of how architectural choices in C-SLAM shape the core trade-offs between *global consistency*, *robot autonomy*, and system performance. To support principled architecture selection, this work aims to quantify and relate key charactersitcs such as latency, scalability limits, robustness and implementation complexity. The key research questions to be addressed are:

1. How do architectures differ in terms of global map update latency and convergence time?
2. What is the impact on latency as the number of collaborating agents increases?
3. What are the computational loads and communication bandwidth requirements of each architecture under varying network constraints, and how do these evolve under constrained network conditions?
4. How does the choice of architecture affect the system's robustness to common real-world challenges?

# 4 Structure of the Thesis

This thesis is organised into six chapters. Chapter 2 introduces the fundamental concepts of graph based SLAM and C-SLAM, establishing the theoretical basis for the subsequent analysis. Chapter 3 reviews the state of the art in collaborative SLAM and builds a comparative analysis grounded in existing literature. Chapter 4 outlines the structure of the comparative framework and the design of the simulation-based evaluation strategy. Chapter 5 details the implementation of the experimental testbed, including the deployment of representative collaborative SLAM architectures. Chapter 6 presents and analyses the comparative results with respect to performance, latency, resource utilisation, and robustness. Finally, Chapter 7 summarises the key findings, draws conclusions, and discusses directions for future research.

# 2

# Fundamentals of SLAM and Collaborative SLAM

## 1 Single-Agent SLAM

Simultaneous Localisation and Mapping (SLAM) is a state estimation problem in which an agent or a mobile robot is tasked to build a map of an unknown environment while simultaneously localising itself within that map based on on-board sensor measurements [12, 1]. At the start of a mission, the robot has no prior knowledge of its environment, and its initial pose defines the coordinate frame of reference. As the robot moves, it measures and maps the environment with reference to this initial position, therefore making the process of mapping incremental in nature. However, inaccuracies in the robot's movement lead to an increasing deviation from the true position, potentially degrading the map quality. To counteract this, the robot needs to consistently optimise its estimated trajectory and map representation through techniques such as sensor fusion, loop closure detection, and nonlinear optimisation, thereby minimising accumulated error and improving overall accuracy.

Modern SLAM systems address this challenge by fusing heterogeneous sensor data (e.g., wheel odometry, inertial measurements, cameras, and LiDAR) into a consistent probabilistic estimate of the robot's pose and the surrounding environment. A central idea is to formulate SLAM as an optimisation problem over a set of latent variables (poses and possibly landmarks) that best explain

the observed measurements. This section introduces the standard graph-based formulation that underpins the rest of this research thesis and briefly outlines the typical system architecture of a single-agent SLAM pipeline.

## 1.1 Problem Definition

Let $x_t \in SE(d)$ denote the robot pose at discrete time (or keyframe) index $t$, where $d \in \{2, 3\}$ is the operational dimension and $SE(d)$ is the special Euclidean group. We write a pose as $x_t = (t_t, r_t)$ with translation $t_t \in \mathbb{R}^d$ and orientation $r_t \in SO(d)$, where

$$SO(d) \triangleq \left\{ R \in \mathbb{R}^{d \times d} \;\middle|\; R^\top R = I,\ \det(R) = 1 \right\}. \tag{2.1}$$

Let $m$ denote a map of the environment (e.g., a set of landmarks or a continuous representation). Over a horizon $t = 0, \ldots, T$, the robot receives control inputs $u_{0:T-1}$ and sensor measurements $z_{0:T}$. The probabilistic SLAM problem is to estimate the joint posterior

$$p(x_{0:T}, m \mid z_{0:T}, u_{0:T-1}), \tag{2.2}$$

where $x_{0:T} = \{x_0, \ldots, x_T\}$ denotes the trajectory.

In practice, SLAM backends typically seek a maximum a posteriori (MAP) estimate under modelling assumptions (motion and measurement models, priors, and conditional independence), which yields a sparse optimisation problem (Section 2.1.2). While Eq. (2.2) includes an explicit map variable $m$, this thesis focuses on *pose-graph* formulations where the environment is represented implicitly through relative constraints and the backend optimises over poses only. This choice matches the backend-centric scope of the thesis and the experimental setup introduced in Chapter 4.

## 1.2 Graph-Based SLAM Framework

Graph-based SLAM represents the estimation problem as a sparse graphical model where nodes correspond to unknown variables (robot poses and, optionally, landmarks), and edges correspond to probabilistic constraints derived from sensor measurements. In the SLAM literature, such edges are commonly referred to as *factors* [12]. Throughout this thesis, the terms *factor* and *constraint* are used interchangeably, both denote a measurement-derived relationship between a subset of state variables.

In the remainder, discrete keyframes/poses are indexed by $i, j$, and reserve $t$ for time.

#### *Constraints as pairwise factors*

The pose-graph setting used here is naturally expressed in terms of pairwise constraints between poses. Let $\mathcal{Z}$ denote the set of relative-pose measurements and let $\mathcal{E}$ denote the set of constrained pose index pairs $(i, j)$. Each measurement

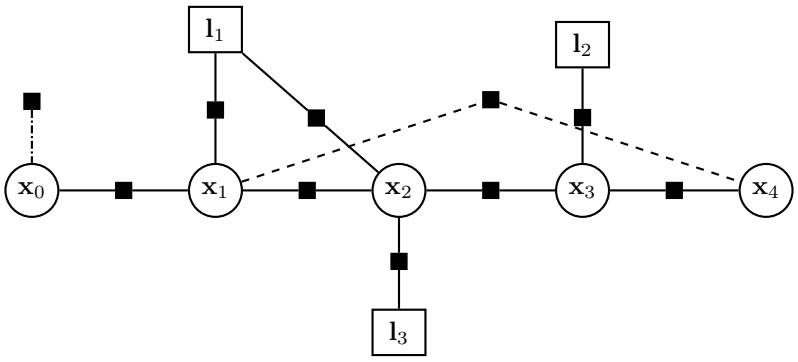


Figure 2.1: Bipartite factor-graph representation of SLAM: circular pose nodes $\mathbf{x}_t$, rectangular landmark nodes $\mathbf{l}_i$, and square factor nodes (black) encoding constraints through different edge types (odometry, landmark observations, loop closures, prior).

$z_{ij} \in \mathcal{Z}$ induces a likelihood term (factor) connecting two pose variables $x_i$ and $x_j$:

$$f_{ij}(x_i, x_j) \propto \exp\left(-\frac{1}{2} \left\| z_{ij} - h(x_i, x_j) \right\|^2_{\Omega_{ij}}\right), \tag{2.3}$$

where $h(x_i, x_j)$ predicts the relative transformation implied by the current pose estimates and $\Omega_{ij}$ is the information matrix (inverse covariance) weighting the residual. The Mahalanobis norm is

$$\|e\|^2_{\Omega_{ij}} \triangleq e^\top \Omega_{ij} e. \tag{2.4}$$

Conceptually, $z_{ij}$ encodes "what the sensors say" about the relative pose between two states (e.g. odometry between consecutive keyframes, or a loop closure between revisited places). The function $h(\cdot)$ encodes "what the current state estimate predicts" for the same relative relation.

Typical constraint types in pose-graph SLAM include:

- **Motion constraints** between consecutive keyframes (short-horizon odometry / scan matching / IMU-derived relations),
- **Intra-robot loop closures** between non-consecutive poses when the robot revisits a place, and
- **Prior constraints** that anchor otherwise unobservable degrees of freedom (to resolve gauge freedom).

*Nonlinear least-squares optimisation template*

Under standard conditional-independence assumptions, the posterior over the unknown variables can be factorised into a product of likelihood and prior terms,

which is naturally represented as a factor graph (Section 2.1.2). For a generic set of factors $\{\phi_k\}$, each involving a subset of variables $X_k \subseteq X$, we write

$$p(X \mid \mathcal{Z}) \propto \prod_k \phi_k(X_k). \tag{2.5}$$

Assuming independent, zero-mean Gaussian noise models, each factor can be expressed in exponential form and MAP estimation reduces to a nonlinear least-squares (NLLS) problem:

$$X^\star = \arg\min_X \sum_k \|e_k(X_k)\|^2_{\Omega_k}, \tag{2.6}$$

where $e_k(\cdot)$ is the residual induced by factor $k$ and $\Omega_k$ is the corresponding information matrix.

A particularly important special case for this thesis is *pose-graph SLAM*, in which all factors are (typically) pairwise relative-pose constraints between pose variables. Let $\mathcal{E}$ denote the set of constrained index pairs $(i, j)$ and let $z_{ij}$ be the corresponding relative measurement. The canonical pose-graph objective becomes

$$X^\star = \arg\min_X \sum_{(i,j)\in\mathcal{E}} \|z_{ij} - h(x_i, x_j)\|^2_{\Omega_{ij}}. \tag{2.7}$$

Equation (2.7) is the *reference optimisation template* used throughout this thesis. Later chapters specialise it to multi-robot pose graphs, and the implementation chapters show how different backends solve the same objective under different communication and computation constraints.

*Solving the optimisation problem*

The objective in Eq. (2.7) is nonlinear because poses live on a manifold and relative-pose prediction involves nonlinear composition. Backends therefore solve it iteratively by linearising residuals around a current estimate and computing an incremental update.

Let $\delta$ denote a local perturbation in a tangent space and let $\oplus$ denote a retraction operator that maps a perturbation back to the manifold. Linearising a residual term yields

$$\big(z_{ij} - h\big((x_i \oplus \delta_i), (x_j \oplus \delta_j)\big)\big) \approx (z_{ij} - h(x_i, x_j)) + J_{ij}\,\delta, \tag{2.8}$$

with Jacobian $J_{ij}$ evaluated at the current estimate. Stacking all terms produces a sparse linear least-squares problem in $\delta$, which can be solved efficiently using sparse factorisation. In practice, Gauss–Newton or Levenberg–Marquardt variants are used.

Two solver styles are common:

- **Batch optimisation**, which periodically relinearises and solves the full problem, and

- **Incremental optimisation**, which updates the solution efficiently as new factors arrive.

Incremental smoothing and mapping methods (e.g. iSAM2) exploit the sparsity structure to update factorisations efficiently and are well suited to the streaming factor setting used in this thesis (see Chapter 5, centralised backend).

## 1.3 SLAM System Architecture

While the graph-based formulation defines the underlying estimation problem, practical SLAM systems are organised as modular pipelines that process sensor data in real time. A widely adopted abstraction is the division into a *frontend*, which processes raw sensor data and proposes constraints, and a *backend*, which maintains and optimises the factor graph [12]. Figure 2.2 conceptually illustrates this split.

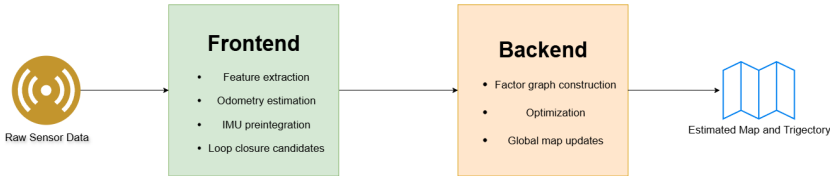


Figure 2.2: Generic SLAM pipeline with frontend and backend.

### *Frontend*

The frontend converts raw sensor streams into a compact set of geometric and topological constraints. Its typical responsibilities include:

- **Preprocessing and calibration:** Synchronisation of multi-sensor data, undistortion of images, and application of extrinsic and intrinsic calibration.
- **Motion estimation:** Computation of relative pose estimates between consecutive frames or scans using visual odometry, LiDAR odometry, or IMU preintegration.
- **Feature extraction and matching:** Detection and description of salient features (e.g. keypoints, edges) and data association across observations.
- **Keyframe selection:** Sub-sampling of frames or scans to maintain a tractable problem size while preserving geometric coverage.
- **Outlier rejection and place recognition:** Application of geometric consistency tests (e.g. RANSAC, epipolar constraints) and appearance-based retrieval (e.g. bag-of-words, deep embeddings) to filter spurious matches and propose candidate loop closures.

The primary output of the frontend is a set of candidate factors that can be added to the factor graph for the backend optimisation. The frontend does not guarantee long-term global consistency and its estimates are prone to drift.

#### *Backend*

The backend maintains the current factor graph and computes the robot trajectory and map estimates by solving Eq. (2.7). Its responsibilities typically include:

- **Graph management:** Inserting new nodes and factors as they are proposed by the frontend, and optionally marginalising or pruning variables to control computational complexity.
- **Optimisation scheduling:** Deciding when to trigger incremental updates versus more expensive batch re-optimisations, trading off accuracy and latency.
- **Linearisation and solving:** Building and solving the linearised normal equations using sparse matrix factorisation or incremental factorisation updates.
- **State dissemination:** Providing updated pose and map estimates to downstream components such as control, planning, or visualisation.

#### *Intra-Robot Loop Closure*

As the robot explores, its trajectory may revisit previously mapped areas. Detecting such events is known as *loop closure detection*. A constraint is added between non-consecutive poses $(i, j)$. In the single-robot setting, such a constraint is called an *intra-robot loop closure*. Loop closures are crucial as they introduce long-range information that corrects accumulated drift and improves global consistency.

# 2 Collaborative SLAM

Collaborative SLAM *(C-SLAM)* generalises SLAM to a team of robots that exchange information to jointly estimate their trajectories and (implicitly or explicitly) a shared map [1, 6]. From an estimation perspective, the extension is rather simple, the variable set grows from one trajectory to multiple trajectories, and additional inter-robot constraints couple those trajectories but from a systems perspective, the extension becomes tedious as communication bandwidth, latency, temporary partitions, and compute limitations constrain how the global optimisation problem can be represented and solved in practice.

## 2.1 Multi-robot state and pose graph

Consider a team of $N$ robots. For each robot $r \in \{1, \dots, N\}$, let $T_r$ denote the index set of keyframes (pose nodes) associated with that robot, and let $x_i^{(r)}$ denote the pose of robot $r$ at keyframe $i \in T_r$. The global multi-robot state is the set of all poses across all robots:

$$X = \left\{ x_i^{(r)} \;\middle|\; r \in \{1, \dots, N\},\, i \in T_r \right\}. \tag{2.9}$$

The measurement set $\mathcal{Z}$ contains relative pose constraints within each robot and across robots. The corresponding edge set $\mathcal{E}$ can be conceptually decomposed into:

- **Local edges** (within a robot): odometry and intra-robot loop closures, and
- **Inter-robot edges** (across robots): constraints connecting $x_i^{(r)}$ and $x_j^{(s)}$ with $r \neq s$.

while the optimisation objective remains the same as in the single-robot case that is to estimate $X$ so that all relative constraints are satisfied as well as possible. The difference is that the graph now consists of multiple per-robot subgraphs connected by a set of inter-robot edges.

## 2.2 Inter-robot loop closures

In addition to intra-robot loop closures, multi-robot systems form *inter-robot loop closures* when different robots observe common structure or each other. These events introduce constraints between poses belonging to different robots, i.e. factors connecting $(x_i^{(r)}, x_j^{(s)})$ with $r \neq s$. Inter-robot loop closures are particularly valuable because they align local frames and correct drift between agents, enabling a globally consistent multi-robot estimate.

## 2.3 Architectural Classes for Collaborative SLAM

The factor-graph formulation above describes a conceptually centralised optimisation problem over all robots and landmarks. However, implementing a fully centralised solution is often impractical due to communication bandwidth limits, latency constraints, and the desire for robustness to node failures. Consequently, a wide range of C-SLAM architectures has been proposed, which can be broadly classified into *centralised*, *decentralised*, and *hybrid or hierarchical* designs [1, 6]. Figure 2.3 illustrates these high-level classes.

### *Centralised Architectures*

In a centralised C-SLAM architecture, a dedicated server (or backend node) collects information from all robots and performs the global optimisation. Each

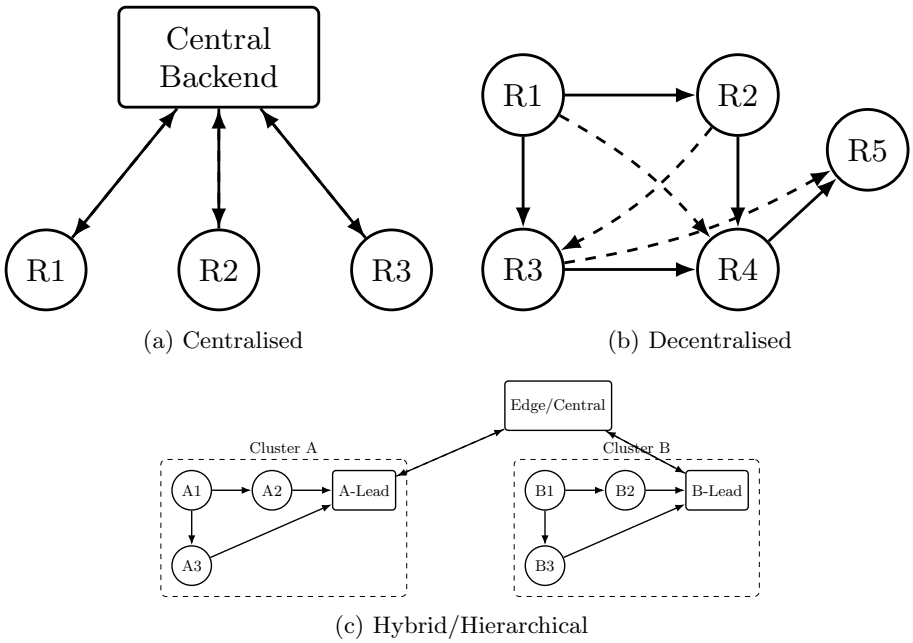


(a) Centralised

(b) Decentralised

(c) Hybrid/Hierarchical

Figure 2.3: Collaborative SLAM architectures: centralised, decentralised, and hybrid/hierarchical.

robot typically runs a lightweight local frontend that estimates its own motion and detects intra-robot loop closures. The robots then transmit summarised information (e.g. pose graph constraints, keyframes, or local maps) to the central server, which maintains a global factor graph and periodically computes a joint estimate of all robot trajectories and the environment.

***Decentralised Architectures***

Decentralised C-SLAM architectures avoid a dedicated central server. Instead, each robot maintains its own local factor graph and collaborates with other robots by exchanging selected information with peers. Inter-robot loop closures are discovered through communication (e.g. exchange of descriptors or keyframes), and the corresponding constraints are incorporated into each robot's local optimisation. Some systems employ consensus or distributed optimisation algorithms to ensure that the local estimates converge to a consistent global solution.

***Hybrid and Hierarchical Architectures***

Hybrid or hierarchical architectures combine elements of centralised and decentralised designs. For example, robots may form clusters, each with a cluster head that aggregates local information and communicates with other cluster heads

or a higher-level server. Alternatively, certain tasks (such as place recognition or map compression) may be centralised, while local trajectory optimisation remains on-board.

# 3

# State of the Art

This chapter reviews representative C-SLAM systems with emphasis being placed on *backend optimisation and communication semantics* because these are the dimensions that most clearly differentiate centralised and decentralised designs while remaining comparable across sensor modalities.Broad surveys such as [1, 18, 4] cover the wider design space. The chapter is intentionally structured around the evaluation dimensions that later become first-class response variables: global consistency and accuracy, correction latency, bandwidth and communication structure, scalability with team size, and robustness under degraded networking.

## 1 Centralised C-SLAM

### 1.1 Architectural patterns

Early work such as $C^2TAM$ [22] demonstrated the motivation for centralisation where computationaly expensive mapping and optimisation can be offloaded to infrastructure, enabling lightweight agents to perform real-time tracking while still benefiting from global refinement. Related server-backed frameworks, such as the multi-robot pose-graph server in [10], similarly highlight that central infrastructure can merge local maps even when robots do not share an initial global frame, provided inter-robot correspondences (e.g. visual loop closures) are available.

A recurring pattern in modern centralised systems is the separation of *local autonomy* from *global consistency*. In *CCM-SLAM* [24] and *CVI-SLAM* [14], each robot runs its local estimation loop continuously, while the server performs map merging and optimisation and returns drift-corrected poses. This design is attractive in practice because it degrades gracefully when communication is intermittent, local tracking continues, and global corrections are incorporated when connectivity becomes available again.

*COVINS* [25] advanced this approach; a central "map manager" receives keyframes from multiple agents and uses a unified place recognition pipeline (based on bag-of-words *(BoW)*) to detect both loop closures and inter-agent map overlaps. The server performs continuous pose graph optimisation and schedules full bundle adjustment periodically, balancing global consistency with real-time responsiveness. *COVINS-G* [21] generalises the same backend concept to accept heterogeneous frontends, which is a practical requirement in multi-robot teams where sensing stacks and odometry quality may differ across agents.

A second recurring pattern is *communication-aware summarisation*. Centralised systems rarely stream raw sensor data; instead, they transmit sparse keyframes, compact descriptors, downsampled point clouds, or selectively offloaded subsets of observations, and the server returns comparatively small correction messages (e.g. optimised poses). Multi-modal systems show that the same principle extends beyond vision. *LAMP 2.0* [2] targets GPS-denied subterranean environments and integrates heterogeneous robots with a robust centralised backend. *CoLRIO* [32] combines LiDAR-inertial odometry with UWB ranging and sends downsampled point clouds, IMU pre-integrations, and range measurements to a central factor-graph optimiser. *AdaptSLAM* [5] makes the communication policy explicit by using an uncertainty-based rule to decide which keyframes to transmit, effectively treating bandwidth as a controllable resource.

## 1.2 Performance implications

Centralised optimisation over all agents' constraints tends to yield strong global consistency because the server can jointly exploit multi-view observations and inter-robot loop closures to correct drift that is unobservable from any single trajectory. This effect is visible in vision-centric systems such as *COVINS* [25] and in multi-modal fusion systems such as *CoLRIO* [32], where additional cross-robot constraints (e.g. UWB ranging) directly improve localisation in degraded visual conditions. Central servers can also apply computationally intensive refinement steps (e.g. periodic bundle adjustment in visual(-inertial) pipelines), which may be infeasible on resource-constrained robots.

Reported quantitative results illustrate these benefits, but remain difficult to compare directly across papers due to differing datasets, sensing stacks, and evaluation protocols. For instance, *COVINS* reports centimetre-level trajectory errors and low scale drift on EuRoC benchmarks [25], while *CoLRIO* reports that adding UWB ranging improves accuracy in degraded conditions (e.g. reducing ATE from 0.32 m to 0.23 m over 100 m trajectories) [32]. Central aggregation is

also particularly attractive for dense or shared reconstructions, where exchanging raw depth or point-cloud content peer-to-peer is impractical; systems such as *CCMD-SLAM* exemplify this direction [36].

At the same time, the literature converges on two limitations of the client–server paradigm. First, scalability is constrained by server computation and aggregate uplink bandwidth. As team size and map size grow, the server must ingest more keyframes, run more place recognition, and optimise a larger pose graph. Second, correction latency becomes a system-level variable, loop closures and global corrections are applied after a communication-and-optimisation cycle, so robots operate on local odometry between correction updates. This is not necessarily problematic, but it creates a trade-off between "how often to optimise and broadcast" and "how much bandwidth and compute to spend", which is precisely the kind of trade-off that motivates controlled evaluation.

Reported communication characteristics in centralised systems also illustrate the typical asymmetry. For instance, *COVINS* reports keyframe transmission at 5 Hz and pose-correction return messages at 2 Hz, with an uplink bandwidth on the order of hundreds of kB/s per agent (reported around ∼493 kB/s) and a much smaller downlink for corrections (reported around ∼2.3 kB/s) [25]. LiDAR-centric systems such as *CoLRIO* report higher per-keyframe payloads due to point-cloud components (e.g. ∼242 kB keyframes and ∼600 kB/s per robot), yet still rely on downsampling and selective transmission to keep traffic manageable [32]. These figures are not directly comparable across papers because datasets, sensing stacks, and implementation details differ; nevertheless, they consistently show that centralised designs depend on sustained uplink capacity and that server-side processing time and network conditions jointly shape correction delays.

# 2 Decentralised/Distributed Collaborative SLAM

## 2.1 Architectural patterns

The foundational distributed factor-graph architecture was established by *DDF-SAM* [8, 7], which formalised how local estimation problems can be coupled through selective factor exchange while preserving autonomy. Contemporary systems such as *DCL-SLAM* [33] and *Swarm-SLAM* [16] build on this principle by making collaboration opportunistic where agents exchange information with neighbours when connectivity is available, without requiring persistent global communication.

Because decentralised systems cannot rely on a high-capacity uplink to a server, they tend to treat bandwidth as a primary design constraint. Visual systems such as *Data-Efficient Decentralised V-SLAM* [6] pioneered a two-stage protocol in which robots first exchange compact descriptors to propose candidate loop closures and transmit heavier keyframe data only when a promising correspondence is detected. *DOOR-SLAM* [17] follows the same idea and focuses on sharing only the information required for inter-robot loop closures, combined with explicit consistency filtering. *Kimera-Multi* [3, 30] similarly leverages compact

bag-of-words descriptors and sparse representations during robot rendezvous, enabling robust place recognition without continuous large data exchange.

LiDAR-centric decentralised systems adopt analogous strategies. *DCL-SLAM* [33] employs lightweight LiDAR descriptors such as LiDAR-Iris and shares keyframe scans and loop constraints on demand rather than continuously. *Swarm-LIO2* [34] is designed for UAV swarms and broadcasts minimal state packets (identity, current pose, mutual observations), enabling plug-and-play collaboration under strict bandwidth budgets. *D*$^2$*SLAM* [31] introduces an adaptive policy that distinguishes near-field and far-field collaboration. Nearby agents exchange richer information for high-accuracy fusion, while distant agents receive compressed summaries to preserve scalability.

A second cornerstone is *distributed optimisation and outlier rejection*. Without central arbitration, incorrect inter-robot loop closures can corrupt the estimate unless filtered robustly. *Kimera-Multi* couples collaboration with robust block coordinate descent (RBCD) for distributed pose-graph optimisation and employs a max-clique-based strategy to filter inconsistent loop closures. Several systems incorporate explicit geometric consistency checks such as PCMS (e.g. *DOOR-SLAM* [17] and *DCL-SLAM* [33]) to validate inter-robot loop closures locally before accepting them into the distributed optimisation. These verification steps are not optional details: they are core enablers of decentralisation because communication is asynchronous and incorrect constraints cannot be "fixed" by a single trusted server.

## 2.2 Performance implications

Decentralised systems avoid a single network bottleneck and can achieve low front-end latency because odometry and local estimation remain onboard. The trade-off is that global consistency is reached through iterative exchange and distributed optimisation rather than a single joint solver step. For example, *D*$^2$*SLAM* reports visual-inertial odometry and loop closure processing below 20 ms per frame on standard hardware [31], while *Kimera-Multi* reports that its distributed optimiser can provide rapid approximate solutions and higher-quality solutions with longer convergence times [3]. Such results illustrate a general property of decentralised backends that the time-to-global-consistency depends on both the optimisation schedule and the communication opportunities between agents.

In return, decentralised architectures can drastically reduce communication requirements through selective exchange. *Data-Efficient Decentralised V-SLAM* transmits compact descriptors first (reported around $\sim$200 B) and sends full keyframes only when necessary (reported $\sim$50–100 kB), yielding large reductions relative to naive keyframe broadcasting [6]. *DOOR-SLAM* reports similarly compact inter-robot exchanges when a loop closure is confirmed and filtered (reported $< 20$ kB per successful exchange) [17]. Swarm-scale systems emphasise minimal packet designs. *Swarm-LIO2* targets per-agent traffic below 10 kB/s [34], and *D*$^2$*SLAM* distinguishes near-field sharing of richer packets (reported $\sim$100 kB keyframes) from far-field sharing of compressed summaries to preserve scala-

bility [31]. These reported behaviours consistently indicate that decentralised systems can bound bandwidth usage, at the cost of higher onboard computation and more complex coordination and verification protocols.

# 3 Comparative synthesis

The state of the art portrays centralised and decentralised C-SLAM as two ends of an architectural spectrum, with hybrid methods interpolating between them [16, 31, 5]. From the perspective of this research thesis, the key point is that performance differences are not purely algorithmic; they are emergent properties of how optimisation, communication, and system scheduling interact. Table 3.1 lists key characterstics that enable comparission between the architectures.

| **Dimension** | **Centralised SLAM** | **Decentralised SLAM** |
|---|---|---|
| **Global Accuracy** | High | Moderate to High |
| **Latency** | Higher (offloaded to server) | Lower (local) |
| **Scalability** | Limited by server capacity and bandwidth bottleneck | Scales with team size; depends on network topology |
| **Communication** | High uplink; asymmetric patterns | Low; bounded; peer-to-peer |
| **Robustness** | Central server as single point of failure | High resilience; graceful degradation with robot failures |

Table 3.1: Comparison of centralised and decentralised C-SLAM architectures. These trends are consistent across visual, LiDAR, and multi-modal systems.

Despite extensive research, three limitations recur across published C-SLAM systems.

**(1) Limited controlled comparison across architectures.** Most papers demonstrate a single pipeline end-to-end and compare against baselines that differ in more than one aspect (frontend, sensing, map representation, compute platform, or parameterisation). As a result, it is difficult to attribute observed performance differences to the architectural variable itself rather than to confounding factors.

**(2) Networking is usually a background assumption rather than a first-class experimental factor.** While many systems motivate their design via bandwidth reduction or resilience to intermittent links, evaluations often assume good connectivity or report results without systematic control of packet loss, added latency, bandwidth caps, or temporary partitions. Consequently, it remains unclear how robust different backends are under realistic communication stressors and how correction latency depends on network conditions.

**(3) Metrics and reporting are fragmented.** Accuracy is typically reported (e.g. ATE), but latency, bandwidth usage, CPU/memory footprints,

and time-to-global-consistency are not consistently measured or defined, and reporting is often system-specific. This makes it difficult to compare approaches or to reason about architectural trade-offs.

These observations motivates a controlled evaluation in which architectural choice is treated as an experimental factor and networking behaviour is explicitly modelled.

# 4

# Methodology

## 1 Experimental Design

This section outlines an experimental research design to evaluate the performance trade-offs between collaborative SLAM backend architectures. A central requirement is that different architectures are assessed under *identical experimental conditions* to ensure a fair, reproducible comparison. The study adopts a controlled, simulation-based methodology in which all pipeline components that are independent of the architectural choice are treated as fixed. Only the *backend optimisation architecture* and its associated *communication semantics* are varied.

In a complete C-SLAM system, each agent would run a local frontend (sensor ingestion, feature extraction/scan matching, local loop closure, and keyframe selection). In this work, frontend processing is abstracted by dataset playback so that backend effects can be isolated without conflating them with frontend design choices.

1. Dataset playback and constraint-stream replay
2. Backend ingestion and optimisation
3. Pose update dissemination
4. Metric logging and post-processing evaluation.

To isolate the effects of architectural selection and structure the evaluation, we define a design space over four groups of experimental variables that capture key dimensions of computation, communication, and environmental variability while remaining abstracted from implementation-specific details:

- *Architecture*: $\mathcal{A}$
- *Team Size*: $\mathcal{N}$
- *Communication Profile (QoS)*: $\mathcal{Q}$
- *Network Impairments*: $\mathcal{I}$

This yields the core experimental design space as the Cartesian product

$$\mathcal{D} = \mathcal{A} \times \mathcal{N} \times \mathcal{Q} \times \mathcal{I}. \tag{4.1}$$

A full combinatorial evaluation over $\mathcal{D}$ would comprise $|\mathcal{A}| \cdot |\mathcal{N}| \cdot |\mathcal{Q}| \cdot |\mathcal{I}|$ conditions, which is computationally expensive. To control the combinatorial growth while maintaining interpretability, a two-stage strategy is adopted:

1. **Baseline Grid**: $\mathcal{Q}$ and $\mathcal{I}$ are fixed to reference settings and compare architectures under clean network conditions. This establishes baseline performance characteristics.
2. **Targeted Sweeps**: By varying one variable group at a time (e.g., $\mathcal{Q}$, $\mathcal{I}$, $\mathcal{N}$) while holding others at baseline. This characterises:
    - *QoS sensitivity:* how delivery guarantees and history settings affect latency, reliability, and stability
    - *Network robustness:* response to packet loss, delay, bandwidth constraints, and temporary partitions
    - *Scalability with team size:* effects of increasing the number of agents on coordination and computational load

# 2 State Representation and Estimation Variables

To compare backend architectures under a *fixed* estimation problem, all systems in this thesis solve the same pose-graph maximum-likelihood objective and differ only in how optimisation and information exchange are realised. We adopt the factor-graph formulation and the generic NLLS template from Chapter 2 (Section 2.1.2 and Eq. (2.6)) and instantiate it here to the specific multi-robot, pose-only setting used in the experiments.

## 2.1 Pose variables

Each robot maintains keyframe poses $x_i^{(r)} \in SE(d)$ with $d \in \{2, 3\}$ depending on the dataset. A pose is written as $x = (t, r)$ with translation $t \in \mathbb{R}^d$ and orientation $r \in SO(d)$; the manifold notation and parameterisations are introduced in Section 2.1. In the implementation, orientations may be stored in an equivalent representation (e.g., quaternions for $SO(3)$), but the estimation problem is defined on $SE(d)$.

## 2.2 Multi-robot global state

Consider a team of $N$ robots. For robot $r \in \{1, \dots, N\}$, let $T_r$ denote the index set of keyframes (pose nodes) used by the backend, and let $x_i^{(r)}$ be the pose of robot $r$ at keyframe $i \in T_r$. The global pose-graph state is the set of all robot poses

$$X = \left\{ x_i^{(r)} \;\middle|\; r \in \{1, \dots, N\},\, i \in T_r \right\}. \tag{4.2}$$

All architectural variants considered in this work operate on the same conceptual state $X$; differences arise from how $X$ is partitioned, updated, and synchronised.

## 2.3 Constraint sets and pose graph

The frontend (or, in this experimental setup, dataset playback) provides relative-pose constraints between keyframes. We distinguish:

- **Odometry / motion constraints** between successive keyframes on each robot, collected in $\mathcal{E}_{\text{odo}}$,
- **Intra-robot loop closures** within a robot's trajectory, collected in $\mathcal{E}_{\text{intra}}$, and
- **Inter-robot loop closures** coupling poses across robots, collected in $\mathcal{E}_{\text{inter}}$.

The full edge set is their union $\mathcal{E} \triangleq \mathcal{E}_{\text{odo}} \cup \mathcal{E}_{\text{intra}} \cup \mathcal{E}_{\text{inter}}$, optionally augmented with a unary *anchoring* factor on a designated reference pose to remove gauge freedom.

Each constraint $(i, j) \in \mathcal{E}$ is represented by a relative-pose measurement $z_{ij}$ with likelihood

$$f_{ij}(x_i, x_j) \propto \exp\left( -\frac{1}{2} \left\| z_{ij} - h(x_i, x_j) \right\|_{\Omega_{ij}}^2 \right), \tag{4.3}$$

where $h(\cdot)$ predicts the relative transformation implied by the current pose estimates and $\Omega_{ij}$ is the information matrix. The Mahalanobis norm is $\|e\|_{\Omega_{ij}}^2 \triangleq e^\top \Omega_{ij} e$.

### 2.4 Reference optimisation problem

With independent, zero-mean Gaussian noise, maximising the joint likelihood over the pose variables yields the pose-graph NLLS objective. We restate it here in full because it serves as the common reference objective across all architectures in Section 4.3:

$$\hat{\mathcal{X}} = \arg\max_{\mathcal{X}} p(\mathcal{Z} \mid \mathcal{X}) = \arg\min_{\mathcal{X}} \sum_{(i,j)\in\mathcal{E}} \|\mathbf{z}_{ij} - h(\mathbf{x}_i, \mathbf{x}_j)\|^2_{\mathbf{\Omega}_{ij}}, \tag{4.4}$$

where $\mathcal{X}$ denotes the set of pose variables (i.e., $X$ above) and $\mathcal{Z}$ the set of all relative-pose measurements. Compared to the generic template in Eq. (2.6), the "where we change stuff" specialisation is explicit: (i) we estimate a pose-only state (no explicit landmark variables), (ii) we couple robots through $\mathcal{E}_{\text{inter}}$, and (iii) we fix the global reference frame through an anchoring factor.

Equation (4.4) is the estimation problem shared by all pipelines in this thesis; the remaining sections specify how centralised and decentralised backends realise this optimisation under different communication and computation constraints.

# 3 Collaborative SLAM Backend Architectures

Within the experimental design space of Section 4.1, the architectural variable $\mathcal{A}$ has two values: *centralised* and *decentralised*. Both variants aim to solve the same pose-graph objective in Equation (4.4) (a special case of the general template in Chapter 2, Equation 2.7); the comparison therefore isolates *where* optimisation is executed and *what* information is communicated to achieve a consistent estimate. This section specifies how each variant instantiates the backend, including where optimisation is executed and how pose updates and auxiliary information are communicated.

### 3.1 Centralised Collaborative SLAM Backend

In the centralised architecture, a dedicated backend server maintains a single global pose graph over the multi-robot state $X$. Each robot (or a dataset replay process) periodically sends *constraint batches* to the server. These batches contain odometry constraints, intra-robot loop closure constraints, and inter-robot loop closure constraints. The server aggregates the received constraints into one global graph and runs joint pose-graph optimisation over the full state $X$. Where enabled, updated pose estimates are broadcast back to each agent as global state updates. In this work, inter-robot loop closures are treated as precomputed constraints provided by the dataset; data association and loop-closure verification are therefore outside the scope of the backend comparison.

Let $\mathcal{C} \subseteq \mathcal{E}$ denote the set of all intra- and inter-robot constraints that have

been received by the server. The centralised backend solves

$$X^\star = \arg\min_X \sum_{(i,j)\in\mathcal{C}} e_{ij}(X)^\top \, \Omega_{ij} \, e_{ij}(X), \tag{4.5}$$

Equation (4.5) is a special case of Eq. (4.4), where the full edge set $\mathcal{E}$ is replaced by the subset $\mathcal{C}$ available at the server at that time.

where $e_{ij}(X) = z_{ij} - h(x_i, x_j)$ is the residual associated with constraint $(i, j)$ as in Equation (4.3).

## 3.2 Decentralised Distributed SLAM Backend

In the decentralised architecture, no global server exists. Each robot maintains its own local pose graph and participates in a distributed optimisation process via peer-to-peer communication. The objective in Equation (4.4) is the same as in the centralised case, but it is approximated through local computations and information exchange between neighbouring robots.

For robot $r \in \{1, \ldots, N\}$, let

$$G_r = (V_r, E_r) \tag{4.6}$$

denote its local pose graph, where $V_r$ contains the local pose variables $x_i^{(r)}$ for $i \in T_r$ and $E_r$ contains odometry and intra-robot loop closure constraints generated by robot $r$. Inter-robot loop closures introduce cross-graph coupling constraints between robots $r$ and $s$ of the form

$$f_{rs}\big(x_i^{(r)}, x_j^{(s)}\big), \tag{4.7}$$

which connect poses belonging to different local graphs. Using this notation, the global optimisation problem can be written as

$$\min_{\{x^{(r)}\}} \left[ \sum_{r=1}^{N} f_r\big(x^{(r)}\big) + \sum_{(r,s)} f_{rs}\big(x^{(r)}, x^{(s)}\big) \right], \tag{4.8}$$

Equation (4.8) is not a different estimation objective; it is Eq. (4.4) rewritten by grouping terms into per-robot local objectives $f_r(\cdot)$ and cross-robot coupling terms $f_{rs}(\cdot, \cdot)$. Thus, the methodological change from Section 4.3.1 to Section 4.3.2 lies in the computation and communication pattern, while the underlying maximum-likelihood objective remains the same.

where $f_r(\cdot)$ collects all local constraints in $E_r$ and $f_{rs}(\cdot)$ collects all cross-robot coupling constraints between robots $r$ and $s$.

# 4 Communication Model and Network Variables

The backend architectures in Section 4.3 are realised on top of a message-oriented communication layer. This section formalises the communication patterns induced by each architecture and the way network conditions are modelled in the experiments. In the design space $\mathcal{D}$ (Section 4.1), these aspects are captured by the *Communication Profile (QoS)* variable $\mathcal{Q}$ and the *Network Impairments* variable $\mathcal{I}$.

## 4.1 Communication Model

Two distinct communication models are employed, corresponding to the centralised and decentralised backend architectures.

In the centralised configuration, communication follows an asymmetric client-server pattern where all robots transmit constraint batches to the server **(Uplink)**. These batches include odometry constraints and loop closure constraints provided by the dataset (or produced by a frontend in a full system). Where enabled, the server transmits global pose corrections (or updated keyframe poses) back to each robot **(Downlink)**.

In the decentralised configuration, no central server exists and communication is peer-to-peer. Robots exchange interface messages that summarise boundary state estimates (e.g. pose mean and covariance for poses involved in inter-robot loop closures), enabling distributed optimisation without broadcasting a full global state. The communication model is therefore local and topology-dependent.

Messages exchanged in both architectures are timestamped at send and at ingestion time, enabling measurement of end-to-end delays from constraint publication to backend use, as well as message inter-arrival times and effective throughput (bytes per second) per link and per robot. These measurements are used in the evaluation to quantify communication latency and bandwidth usage under different combinations of $\mathcal{A}$, $\mathcal{Q}$, and $\mathcal{I}$.

## 4.2 Network Impairment Model

To evaluate the robustness of collaborative SLAM architectures under adverse communication conditions, controlled network impairments are introduced in the experimental setup. The Network Impairments variable $\mathcal{I}$ parameterises the following impairment types:

- **Stochastic loss**: Messages are randomly dropped according to a specified loss rate, modelling unreliable links and congestion.
- **Burst loss**: Messages are dropped in periodic bursts, modelling transient interference and contention.
- **Blackouts / partitions**: Scheduled sender or receiver blackouts emulate temporary disconnections (including asymmetric communication failures).

- **Bandwidth caps**: Per-sender throughput limits are enforced via token-bucket shaping, which introduces send delays consistent with a constrained channel.

Impairments are applied in a controlled and repeatable manner by a network emulation layer at message send time. For a given impairment configuration $\mathcal{I}$, the same impairment parameters are applied across both architectures to ensure architectural fairness.

In practice, the impairment mechanism supports different *application modes* depending on which communication edges are being studied: impairments can be applied to (i) the factor-publisher uplink (constraint availability), (ii) backend-internal communication (decentralised peer-to-peer interface exchange and/or centralised map downlink), or (iii) both. Fair comparisons therefore condition on a fixed impairment mode and parameter set, and results are interpreted accordingly.

By combining the communication models of Section 4.4.1 with the impairment levels defined here, the experimental framework systematically explores how architectural choices ($\mathcal{A}$) interact with QoS settings ($\mathcal{Q}$) and network impairments ($\mathcal{I}$) in terms of latency, communication load, scalability, and estimation accuracy.

# 5 Performance Metrics

For each experimental configuration in the design space $\mathcal{D}$, a set of response variables is evaluated to capture system performance in terms of latency, estimation accuracy, and resource usage. These metrics provide the quantitative basis for comparing centralised and decentralised architectures under varying team sizes and network conditions. The metrics are grouped into three categories: *Timing metrics*, *Accuracy metrics* and *Resource metrics*.

## 5.1 Timing Metrics

Timing metrics quantify (i) how quickly a backend incorporates newly ingested constraints and (ii) how quickly corrections become visible to the team. To make compute time and dissemination time comparable across architectures, we distinguish backend solve latency from (optional) update broadcast latency.

**Ingest-to-optimisation latency $L_{\mathbf{opt}}$.** For the centralised backend, where each ingest event corresponds to a clearly defined server-side batch, we additionally report the elapsed time between ingestion of a constraint batch and completion of the corresponding optimisation update:

$$L_{\text{opt}}(b) = t_{\text{optimization\_end}}(b) - t_{\text{ingest}}(b), \tag{4.9}$$

where $t_{\text{ingest}}(b)$ is the timestamp at which the backend accepts batch $b$ and $t_{\text{optimization\_end}}(b)$ is the timestamp at which the optimisation update that incorporates $b$ completes. For decentralised runs there is no single, architecture-

agnostic notion of "backend ingest of batch $b$" because each agent ingests both local factors and asynchronous peer updates; in this thesis we therefore treat ingest-to-optimisation as architecture-specific and rely on $D_{\text{opt}}$ as the cross-architecture compute indicator.

**Ingest-to-broadcast latency $L_{\text{global}}$ (centralised runs).** For the centralised architecture, the server may additionally publish a global update (map downlink) to make the updated state available to robots. The corresponding dissemination latency is defined as

$$L_{\text{global}}(b) = t_{\text{broadcast}}(b) - t_{\text{ingest}}(b), \tag{4.10}$$

where $t_{\text{broadcast}}(b)$ denotes the time at which the updated state is published. In decentralised runs there is no single broadcast event; therefore $L_{\text{global}}$ is not defined and settling behaviour is characterised via stabilisation-based metrics ($T_{\text{LC}}$ and $T_{\text{conv}}$).

**Stabilisation criterion.** Several timing KPIs require a backend-agnostic notion of "the estimate has settled". Let $\mathbf{t}_i^{(u)} \in \mathbb{R}^d$ denote the translation component of pose $x_i$ at backend update/round index $u$. We define the maximum translation change between successive updates as

$$\Delta t_{\max}^{(u)} = \max_i \left\| \mathbf{t}_i^{(u)} - \mathbf{t}_i^{(u-1)} \right\|_2 . \tag{4.11}$$

Unless stated otherwise, stabilisation is declared when $\Delta t_{\max}^{(u)} \leq \epsilon$ for $S$ consecutive updates, with $\epsilon = 10^{-3}$ and $S = 3$.

**Loop-closure correction time $T_{\text{LC}}$.** This metric measures how long it takes for an inter-robot loop closure to be reflected in a stable estimate. For a loop-closure event $c$:

$$T_{\text{LC}}(c) = t_{\text{stable}}(c) - t_{\text{det}}(c), \tag{4.12}$$

where $t_{\text{det}}(c)$ is the time at which the loop-closure constraint is ingested and $t_{\text{stable}}(c)$ is the timestamp of the first update that begins a stable window according to the stabilisation criterion above. This captures both optimisation time and (where applicable) communication delays for the correction to propagate.

**Time-to-convergence $T_{\text{conv}}$.** For long runs, we measure the time required for the system to reach a globally stable pose graph under the same stabilisation criterion. Let $u^\star$ be the first update index at which $\Delta t_{\max}^{(u)} \leq \epsilon_{\text{conv}}$ holds for $S$ consecutive updates. The time-to-convergence is then

$$T_{\text{conv}} = t(u^\star) - t_{\text{start}}, \tag{4.13}$$

where $t(u^\star)$ is the timestamp of the first stable update and $t_{\text{start}}$ is the start time of the run. Unless stated otherwise, we use $\epsilon_{\text{conv}} = 10^{-3}$ and $S = 3$ to match

the KPI derivation implemented in Chapter 5.

## 5.2 Accuracy Metrics

Accuracy is evaluated in terms of both global trajectory consistency and local drift. Absolute Trajectory Error (ATE) and Relative Pose Error (RPE) follow the definitions in [28], for each agent, and aggregate these across the team.

**Absolute Trajectory Error (ATE).** ATE measures the deviation between estimated and ground-truth trajectories after alignment. Because COSMO-Bench provides metric LiDAR trajectories, scale is fixed to $s^* = 1$ and alignment is performed using a rigid transform in $SE(3)$ (rotation $\mathbf{R}^*$ and translation $\mathbf{t}^*$) computed via Umeyama's method. The aligned RMSE ATE for agent $a$ is

$$\mathrm{ATE}^{(a)}_{\mathrm{RMSE}} = \sqrt{\frac{1}{T_a+1}\sum_{k=0}^{T_a}\left\|\mathbf{x}_k^{(a),\mathrm{gt}} - \left(\mathbf{R}^*\mathbf{x}_k^{(a)} + \mathbf{t}^*\right)\right\|_2^2}. \tag{4.14}$$

**Relative Pose Error (RPE).** RPE quantifies local drift between pairs of poses separated by a fixed time interval $\Delta$. For agent $a$, let $\mathbf{t}^{(a)}_{k:\Delta}$ and $\mathbf{t}^{(a),\mathrm{gt}}_{k:\Delta}$ denote the estimated and ground-truth relative translations between times $k$ and $k+\Delta$. The translational component of the relative error is

$$r_k^{(a)}(\Delta) = \left\|\mathbf{t}^{(a),\mathrm{gt}}_{k:\Delta} - \mathbf{t}^{(a)}_{k:\Delta}\right\|_2, \tag{4.15}$$

and the RMSE RPE for agent $a$ is

$$\mathrm{RPE}^{(a)}_{\mathrm{RMSE}}(\Delta) = \sqrt{\frac{1}{T_a-\Delta}\sum_{k=0}^{T_a-\Delta}\left(r_k^{(a)}(\Delta)\right)^2}. \tag{4.16}$$

RPE is evaluated for multiple values of $\Delta$ to capture both short- and long-horizon drift characteristics.

## 5.3 Resource Metrics

Resource metrics assess the computational and communication costs incurred during collaborative SLAM. They are particularly relevant for comparing architectures in terms of scalability and efficiency.

**CPU Utilisation $\rho_{\mathbf{CPU}}$** CPU utilisation is sampled periodically at the process level for the processes involved in each run (e.g. constraint publisher and backend processes). Summary statistics are computed over the evaluation window $[0, T_{\mathrm{eval}}]$, and multi-process backends are reported either per-process or as an aggregate across processes, depending on the available logging.

**Peak Memory Usage $M_{\mathbf{peak}}$** Peak memory usage is defined as the maximum resident set size (RSS) observed during execution for the processes involved in the run. For multi-process backends, the peak can be reported per-process and/or as an aggregate across processes, depending on the available logging.

**Bandwidth Usage $BW$** Bandwidth usage quantifies the total amount of data transmitted per agent over the course of a run. For each agent $a$, we compute

$$BW^{(a)} = \frac{1}{T_{\text{eval}}} \int_0^{T_{\text{eval}}} \sum_c B_c^{(a)}(t)\, dt, \tag{4.17}$$

where $B_c^{(a)}(t)$ is the instantaneous byte rate on communication channel $c$ at time $t$, and $T_{\text{eval}}$ is the evaluation horizon. In practice, this integral is approximated from logged message sizes and timestamps. We additionally report an effective delivery rate, defined as the ratio of successfully received to sent messages, to account for packet loss under impaired network conditions.

Together, these timing, accuracy, and resource metrics provide a multi-dimensional view of system performance, enabling a structured analysis of the trade-offs between centralised and decentralised collaborative SLAM architectures under varying team sizes, QoS settings, and network impairment levels.

# 5

# Implementation

This chapter explains how the experimental methodology is realised in software. The focus is on (i) enforcing a *comparability contract* between architectures by replaying an identical factor stream, (ii) implementing a centralised and a decentralised back end on top of a shared factor representation, (iii) realising controlled communication conditions via ROS 2 QoS and message-level impairments, and (iv) instrumenting the system to produce reproducible KPI logs for the evaluation chapter.

## 1 Dataset and Frontend

A fair architectural comparison requires that both back ends consume an identical frontend output. Although the S3E dataset [11] was initially considered due to its rich multimodal sensing, its computational and storage demands made it impractical for the available experimental setup. More importantly, implementing or modifying a frontend would have introduced additional degrees of freedom that are orthogonal to the architectural research questions.

The `COSMO-Bench` dataset [19] was selected because it provides a standardised collaborative SLAM frontend and a benchmark suite of 24 sequences with annotated intra-/inter-robot loop closures and communication scenarios (Wi-Fi and Pro-Radio). Each sequence is distributed in the JRL (JSON Robot Log) format, which directly encodes the factor stream consumed by both architectures.

**Frontend abstraction.** The "common SLAM frontend" referenced in the methodology (Section 4.1) is instantiated by COSMO-Bench's preprocessing pipeline. Odometry constraints, intra-robot loop closures, and inter-robot loop closures are already detected and validated. The resulting JRL files provide:

- initial pose estimates for all robot keyframes,
- prior factors anchoring each robot's trajectory,
- between-factors for odometry and loop closures (intra- and inter-robot),
- ground-truth trajectories for evaluation,
- optional outlier annotations (not used in the main evaluation unless stated otherwise).

**Comparability contract (fixed frontend).** Both back ends ingest the same JRL factors through the shared loader `c_slam_common/loader.py`. As a result, any measured differences in latency, bandwidth, or estimation behaviour are attributable to the back-end architecture and the configured network conditions, not to differences in frontend processing.

# 2 System Overview

The framework consists of four subsystems: (i) a shared common library for dataset parsing, factor construction, and KPI logging, (ii) a centralised back end implementing global incremental optimisation, (iii) a decentralised back end implementing DDF-SAM-style distributed coordination, and (iv) a ROS 2 middleware layer providing transport, QoS control, and message-level impairments.

The reference implementation targets Ubuntu 22.04 LTS with ROS 2 Humble and Python 3.10. GTSAM ($\geq$ 4.2.0) is used via its Python bindings for factor-graph construction and iSAM2 optimisation. All experiments execute on a single physical machine, while ROS 2 multi-process execution emulates a distributed deployment and allows controlled communication conditions. Executing both architectures on one host introduces an architecture-induced confound: OS scheduling contention (especially in the decentralised multi-process case) can influence wall-clock solver timing; to contextualise timing KPIs, CPU and memory utilisation are sampled and exported alongside evaluation logs (Section 5.7.4).

# 3 Operationalisation of the Experimental Design Space

The experimental design space $\mathcal{D}$ introduced in the methodology (Section 4.1) is instantiated through runtime configuration knobs controlling: back-end architecture, team size, ROS 2 QoS, and network impairments. The implementation

| Path | Purpose |
|---|---|
| `main.py` | CLI entry point: selects back end, dataset, configuration, and output paths |
| `c_slam_common/` | Shared utilities: JRL parsing, factor graph building, noise configuration, KPI/event logging, bandwidth/latency tracking, resource monitoring, helpers |
| `c_slam_central/` | Centralised back end: global iSAM2 optimiser, ROS 2 factor ingestion, optional downlink/ACKs, KPI hooks |
| `c_slam_decentral/` | Decentralised back end: per-agent iSAM2, interface summarisation/exchange, multi-process runner, KPI exports |
| `c_slam_ros2/` | ROS 2 middleware: factor/interface/map messages, QoS configuration, impairment policy, simulation time helpers |
| `tools/` | Orchestration scripts and KPI derivation/export utilities |
| `dataset/` | Example JRL sequences used for development (COSMO-Bench factor streams) |

Table 5.1: Repository layout of the experimental framework.

exposes these knobs via CLI flags and environment variables to enable reproducible sweeps.

**End-to-end run workflow.** A run replays a JRL factor stream over ROS 2 (Subsection 5.3.1) so that both back ends observe the same sequence of priors and between-factors. The selected back end then (i) performs incremental global updates (centralised) or (ii) executes a fixed number of DDF rounds (decentralised), exporting estimates and a timestamped KPI event log. Derived KPIs are computed offline from the event log by `tools/kpi_derive.py`.

**Reproducibility artefacts.** Each run records resolved configuration in `run\_manifest.json`. Orchestrated runs additionally write the resolved orchestrator config and command list (e.g., `orchestrate_config.json`, `orchestrate\_commands.json`) into the export directory, allowing exact reconstruction of command lines and environment variables.

## 3.1 ROS 2 Factor Streaming

A ROS 2 middleware layer emulates real-time factor streaming from each agent without requiring live robots. The factor publisher `tools/ros2\_factor\_publisher.py` publishes per-robot batches on topics `<prefix>/<robot_id>`.

| Design variable | Implementation knobs |
|---|---|
| Architecture $\mathcal{A}$ | `main.py --backend` with values `centralised` or `decentralised`. Orchestrated runs set the same via `tools/orchestrate.py` / `new_eval` configs. |
| Team size $N$ | Derived from the selected JRL sequence: robot IDs are extracted from initialisation blocks (`build_key_robot_map`). The decentralised runner spawns one process per robot (`c_slam_decentral/mp_runner.py`). COSMO-Bench sequences `r3_*`, `r4_*`, `r5_*` realise $N \in \{3, 4, 5\}$. |
| QoS profile $\mathcal{Q}$ | `--qos-reliability`, `--qos-durability`, `--qos-depth`, applied consistently to factor batches, interface messages, and optional downlink (Section 5.6). |
| Impairments $\mathcal{I}$ | JSON profile via `C_SLAM_IMPAIR` or `C_SLAM_IMPAIR_FILE`; instantiated by `ImpairmentPolicy` (`c_slam_ros2/impair.py`) and injected identically across processes. |

Table 5.2: Operationalisation of the design space into concrete runtime knobs.

Batches are JSON-encoded (`c_slam_ros2/factor_batch.py`) and transmitted as `std_msgs/UInt8MultiArray`. Each batch includes lightweight metadata required for instrumentation: `message_id` (UUID), `send_ts_mono` (monotonic timestamp), and `send_ts_wall` (wall-clock timestamp). Robot identity is implied by the topic name and not duplicated in the payload.

**Factor payload** The stream supports `PriorFactorPose3` and `BetweenFactorPose3` objects (rotation, translation, covariance, keys, stamp). These are translated into GTSAM factors by the back-end-specific graph builders. Completion is signalled via `<prefix>/control` messages `DONE:<robot_id>` and a final `DONE_ALL` marker.

# 4 Centralised Back End

The centralised back end aggregates factors from $N$ robots into a single global factor graph and incrementally optimises the joint state using iSAM2. The reference implementation is `c_slam_central/central_backend.py`. Figure 5.1 summarises the interaction between ROS 2 streaming and the central server.

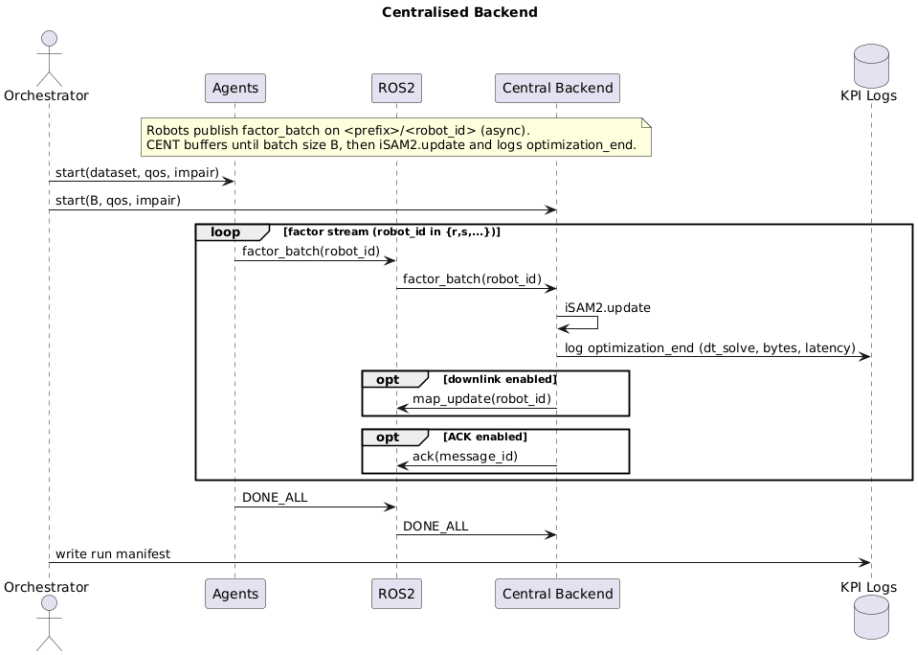


Figure 5.1: Sequence diagram depicting agent–central server interaction.

## 4.1 Input: Factor Ingestion and Batching

The `ROS2FactorSource` (`c\_slam\_ros2/factor\_source.py`) subscribes to `<prefix>/<robot_id>` for all robots. Incoming batches are decoded and annotated with message-level metadata used downstream for KPI logging:

- `__ros2_topic` (source topic),
- `__ros2_msg_bytes` (serialised payload size),
- `__ros2_msg_id` (publisher UUID),
- `send_ts_mono`, `send_ts_wall` (publisher timestamps).

The publisher can bundle multiple factors per ROS 2 message (`--batch-size`). On the server, decoded factors are accumulated until a solver batch threshold is reached (`main.py --central-batch-size`). Each solver batch produces a per-batch graph and initial-value deltas, which are then applied in one iSAM2 update. Ingestion terminates when `DONE_ALL` is received or when an idle timeout expires (`--central-idle-timeout`).

**Initial values.** Initial estimates are obtained from JRL initialisation blocks and stored in `init_lookup`. If a key is missing, the implementation inserts

an identity pose as a fallback and logs a warning, ensuring the graph remains well-formed without factor deferral logic.

## 4.2 Solve: Incremental Optimisation with iSAM2

iSAM2 is configured through `ISAM2Params` in `c_slam_common/isam2.py`. The main exposed knobs are the relinearisation threshold (`--relin-th`) and skip interval (`--relin-skip`). Algorithm 1 summarises the incremental update loop used in the experiments.

**Algorithm 1** Centralised iSAM2 back end: incremental optimisation loop

**Require:** Stream of factors $\mathcal{F}$, initial pose lookup `init_lookup`, batch size $B$
**Ensure:** Global estimate $\hat{X}$

1: Initialise GraphBuilder and iSAM2
2: Accumulate decoded factors into a solver batch of size $B$
3: For each completed batch: build $(G_b, V_b)$ and call iSAM2.update$(G_b, V_b)$
4: On numerical/duplicate-key failure: rebuild iSAM2 from accumulated global graph and retry once
5: After each successful update: extract $\hat{X}$ and emit KPI events for optimisation timing and batch attribution
6: **return** $\hat{X}$

## 4.3 Output: Optional Downlink and ACK Instrumentation

In a deployed centralised system, the server would broadcast the updated global estimate to robots. The framework supports an optional "map downlink" publication (`--emit-map-downlink`) implemented in `c_slam_ros2/map_broadcast.py`. When enabled, downlink traffic is subjected to the same QoS and impairment settings as other topics, and is measured from actual serialised ROS 2 payload sizes.

For delivery-rate diagnostics, optional factor-batch acknowledgements can be enabled (`--emit-factor-acks`). ACK messages bind processed `message_id`s to the solver timeline and allow distinguishing "published" from "observed and processed" traffic under impairments.

**Payload accounting.** For interpretability, the framework may compute a rough lower-bound estimate of the downlink payload assuming binary float64 encoding of pose means (translation + quaternion). However, all reported bandwidth statistics in the evaluation are based on measured serialised message sizes (`__ros2_msg_bytes` and recorded publish sizes), which capture JSON overhead and key strings.

# 5 Decentralised Back End

The decentralised back end implements a DDF-SAM-style distributed optimiser [8, 7]. Each of the $N$ agents maintains a local factor graph and exchanges separator summaries with peers. There is no central coordinator; global consistency emerges through repeated local optimisation and information exchange. Figure 5.2 shows the high-level interaction.

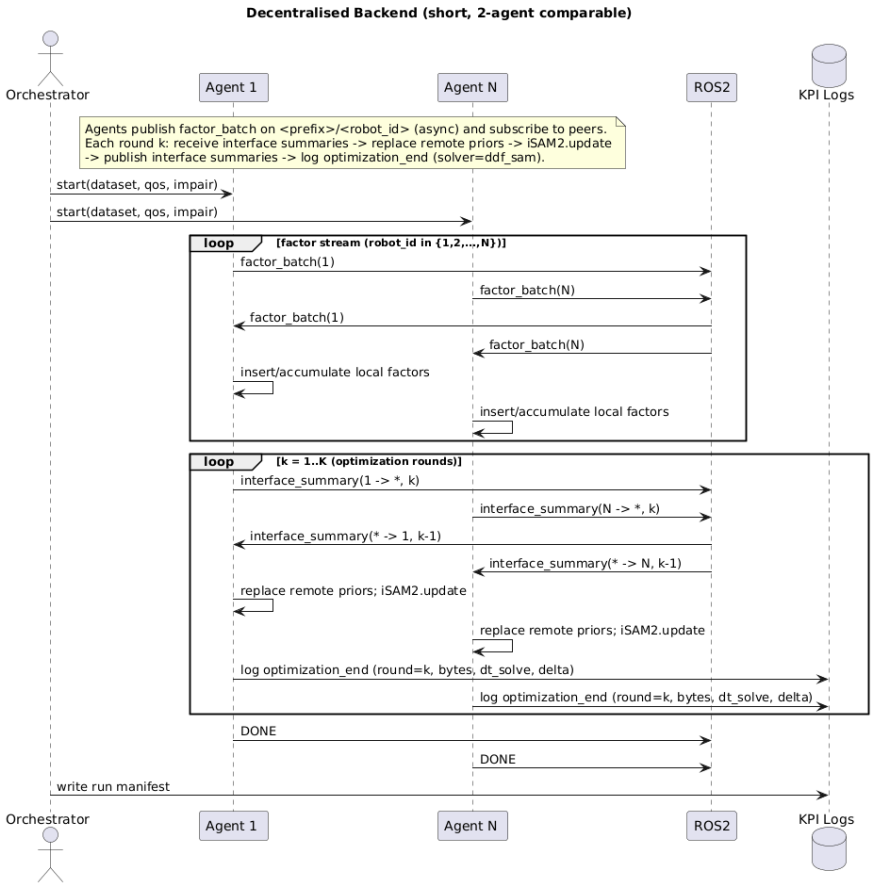


Figure 5.2: Sequence diagram depicting decentralised agent interaction and interface exchange.

## 5.1 Input: Deterministic Factor Partitioning

To ensure reproducibility and avoid double counting, decentralised correctness depends on deterministic factor ownership.

**Key-to-robot mapping.** A global `robot_map` is built once from JRL initialisation blocks using `build_key_robot_map`. All agents share this map to attribute pose keys to robots consistently.

**Inter-robot ownership rule.** For an inter-robot between-factor whose endpoints belong to robots $r$ and $s$, ownership is assigned deterministically:

$$\text{owner\_robot} = \min(r, s).$$

Only the owner inserts that inter-robot between-factor into its local graph. The non-owner couples to the remote endpoint only through separator priors derived from received interface summaries. ROS 2 streaming affects transport only; it does not change the factor classification or ownership logic.

## 5.2 Solve: Local Optimisation and Remote-Prior Refresh

Each agent maintains a persistent local iSAM2 instance (`c_slam_decentral/agents.py`). Static factors (dataset priors, local odometry, local loop closures, and owned inter-robot between-factors) are inserted once. On each coordination round, the agent refreshes time-varying separator priors from the most recently received interface summaries, performs an iSAM2 update, and then summarises its separators for outbound communication.

Algorithm 2 captures the round-level procedure.

**Algorithm 2** Agent round: refresh remote priors, solve locally, and emit separator summaries

**Require:** agent $r$, latest remote summaries, round index $k$
**Ensure:** updated local estimate $\hat{X}_r$ and outgoing interface messages $\mathcal{I}_{out}$

```
Insert static factors into persistent iSAM2 (once)
Build remote separator priors from latest interface messages
Remove previous-round remote priors using removeFactorIndices (if supported)
iSAM2.UPDATE(remote-prior batch graph, remote-prior batch values)
if update fails (indeterminate/duplicate-key) then
    Rebuild iSAM2 from scratch using static factors + owned inter-robot factors + fresh remote priors
end if
X̂_r ← iSAM2.CALCULATEESTIMATE(); emit optimisation KPI events for this round
Compute marginals for communicated separator keys
I_out ← MAKEINTERFACEMSGS(r, X̂_r, marginals)
return X̂_r, I_out
```

**Remote-prior semantics.** Remote separator priors are treated as time-varying "summary constraints" and are replaced each round to avoid accumulat-

ing stale priors. If marginal extraction fails for a separator, the implementation falls back to a conservative diagonal covariance to keep communication and optimisation progressing.

## 5.3 Output: Interface Exchange and Coordination Loop

Agents exchange separator summaries via a peer bus (`c_slam_decentral/communication.py`). Each agent runs in its own OS process via `c_slam_decentral/mp\_runner.py`. Synchronisation is purely message-based (no global scheduler). Each agent iterates a fixed maximum number of rounds and may stop early based on a stability condition.

Algorithm 3 describes the per-agent coordination loop.

**Algorithm 3** Per-agent distributed coordination loop

**Require:** agent $r$, max rounds $R$, tolerances $(\tau_t, \tau_R)$, stable rounds $S$
**Ensure:** final estimate $\hat{X}_r$ and convergence flag
1: Ingest factors for $r$ from `<factor_prefix>/<robot_id>`
2: Initialise peer bus and perform round $k$=0
3: **for** $k = 1$ **to** $R$ **do**
4: Drain inbox; apply latest summaries as remote priors
5: Perform AgentRound and publish fresh interface summaries
6: Update stability counter from interface deltas; stop if stable for $S$ consecutive rounds
7: **end for**

**Convergence monitoring (runtime stop condition).** After each round, an agent compares successive outbound interface states by the maximum translation delta $\Delta t_{\max}$ and maximum rotation delta $\Delta R_{\max}$. Convergence is declared when both fall below thresholds for $S$ consecutive rounds (`--ddf-convergence`, `--ddf-rot-convergence`, `--ddf-stable-rounds`). These checks are local to each agent and may trigger at different round indices due to asynchronous message arrivals. Here, $\Delta t_{\max}$ is computed as the Euclidean norm of the translation difference, and $\Delta R_{\max}$ as the angle (in radians) of the relative rotation between successive quaternion estimates. Independently of this early-stopping rule, each agent enforces a hard maximum of $R$ rounds to bound runtime and ensure experimental reproducibility. A run is marked *converged* only if the stability condition is satisfied before reaching the round budget; otherwise it is treated as not converged within the allocated coordination horizon.

## 5.4 Communication Transport and Message Schema

Interface summaries are encoded as JSON bytes (`c_slam_ros2/interface\_msg.py`) and exchanged via per-receiver ROS 2 topics. For run isolation, the runner appends a unique `run_<id>` namespace to the interface prefix, so agents

publish on `<iface_prefix>/run_<id>/<receiver_id>` and subscribe only to their own receiver topic.

Each interface message contains: `sender`, `receiver`, `key`, `stamp`, pose mean (`translation`, `rotation`), covariance (`covariance`), and the consensus `iteration`. Latency and bandwidth are measured from serialised ROS 2 message payload sizes at publish time (excluding DDS/RTPS and lower-layer overhead); analytical byte counts are not used for evaluation because JSON overhead and string keys are significant and run-dependent.

# 6 Network Impairment and Quality-of-Service Implementation

This section describes how the network conditions from the methodology are realised: impairments are injected at the message level inside the ROS 2 publish paths and are applied consistently across architectures for any chosen impairment *application mode*.

## 6.1 Impairment Injection Points

Impairments are applied in three places:

1. **Factor publisher** (`tools/ros2_factor_publisher.py`): drops/throttles factor batches before publication.
2. **Decentralised peer bus** (`c_slam_decentral/communication.py`): applies the same impairment rules to interface messages.
3. **Central downlink** (`c_slam_ros2/map_broadcast.py`): applies the same rules to optional map updates.

All impairment logic is encapsulated in `ImpairmentPolicy` (`c_slam_ros2/impair.py`) so that a single JSON profile can be injected into all processes by the orchestrator.

## 6.2 Impairment Semantics Relevant to KPIs

The impairment policy combines message drop and delay mechanisms. The details matter because they change how latency and delivery-rate KPIs should be interpreted:

- **Random loss and burst loss** drop messages before they enter the ROS 2 transport.
- **Blackouts** disable send and/or receive for a specified robot over an interval.
- **Bandwidth caps** implement a token bucket that *delays* messages (sleep) to enforce an average throughput, rather than dropping by default.

- **Warmup behaviour** can disable random/burst drops at startup to avoid immediate underconstraint, while still applying bandwidth caps and blackouts.

## 6.3 Impairment Configuration

Impairment profiles are specified as JSON and loaded via `C_SLAM_IMPAIR` (inline) or `C_SLAM_IMPAIR_FILE`. The orchestrator injects the same profile into all processes to ensure that both architectures experience identical impairment settings in comparative runs.

```
{
"seed": 42,
"random_loss_p": 0.05,
"random_warmup_messages": 50,
"burst_period_s": 10.0,
"burst_duration_s": 1.0,
"blackouts": [
{"rid": "r0", "start_s": 30.0, "end_s": 35.0, "mode": "sender"}
],
"bw_caps_mbps": {"default": 2.0, "r1": 1.0},
"warmup_s": 5.0
}
```

## 6.4 Quality-of-Service Configuration

QoS policies (reliability, durability, history depth) are applied consistently to all relevant topics. Controlled sweeps over QoS use `--qos-reliability`, `--qos-durability`, and `--qos-depth`, and the orchestrator forwards the same settings to publisher and solver processes. The baseline profile (`c_slam_ros2/qos.py`) is:

- Reliability: `RELIABLE`
- Durability: `VOLATILE`
- History: `KEEP_LAST` with depth 10

## 6.5 Team Size Scaling and Namespace Isolation

Team size $N$ is determined by the dataset. Factor batches use `<factor_prefix>/<robot_id>` with completion markers on `<factor_prefix>/control`. The decentralised peer bus uses per-receiver topics `<iface_prefix>/run_<id>/<robot_id>`. Sweep runs additionally use `ROS_DOMAIN_ID` isolation to avoid collisions between repeated or concurrent runs.

# 7 Performance Metrics Instrumentation

This section describes how the KPIs defined in the methodology are instrumented in software. The guiding principle is that both architectures emit comparable event streams so that KPI derivation can be performed offline in a back-end-agnostic way where possible.

## 7.1 Event Logging and Derivation Pipeline

All KPI-related measurements are recorded as timestamped events and exported to JSON files under `kpi_metrics/`. The system logs:

- **ingest events** (factor reception and attribution to solver batches/rounds),
- **solver events** (`optimization_start`/`optimization_end` for central batches; per-round solve events for decentralised agents),
- **communication events** (publish sizes for factor batches, interface messages, and optional downlink/ACKs),
- **resource samples** (CPU and memory time series).

Derived KPIs (e.g., stabilisation-based correction times) are computed offline from these event logs by `tools/kpi_derive.py` and written to `kpi_metrics/derived_kpis.json`.

## 7.2 Latency Instrumentation

**Factor-to-solve attribution.** Each ingested factor is assigned to a solver batch (centralised) or to a local optimisation round (decentralised) using the internal batch/round indices emitted by the solver loop. This attribution is what enables ingest-to-optimisation and settling-time KPIs without re-running optimisation offline.

**Timestamps.** Publisher timestamps (`send_ts_mono`, `send_ts_wall`) are carried in the message payload and recorded at reception. Solver timestamps are recorded at optimisation boundaries in the back-end processes. This allows separating transport effects (delays/loss) from solver scheduling effects (batching and compute time). From these event pairs, the evaluation derives explicit latency components, including publish-to-receive $\Delta t_{\text{pub}\to\text{recv}} = t_{\text{recv}} - t_{\text{send}}$, ingest-to-optimisation-start $\Delta t_{\text{ingest}\to\text{opt}} = t_{\text{optimization\_start}} - t_{\text{ingest}}$, optimisation duration $\Delta t_{\text{solve}} = t_{\text{optimization\_end}} - t_{\text{optimization\_start}}$, and settling time as the interval from factor ingestion to the first subsequent optimisation-end event after which estimate changes remain below a stability threshold.

## 7.3 Accuracy Instrumentation

Trajectory accuracy is computed from exported estimates using `c_slam_common/metrics.py`. The implementation performs per-robot alignment against JRL

ground truth and exports ATE/RPE summaries to `kpi_metrics/estimation_metrics.json`. The implementation fixes the similarity scale to $s = 1$ (rigid alignment) because COSMO-Bench trajectories are metric, and reports per-robot RMSE values for evaluation plots.

## 7.4 Resource and Bandwidth Instrumentation

**CPU and memory.** Resource utilisation is sampled using `psutil` (`c_slam_common/resource_monitor.py`). For decentralised runs, the solver aggregates samples across spawned agent PIDs. Summary statistics are exported to `kpi_metrics/resource_profile.json`.

**Bandwidth.** Bandwidth is computed from measured serialised message sizes at publish time. For centralised runs, uplink is the sum of factor batch payload sizes; downlink is measured when enabled. For decentralised runs, bandwidth is derived from outgoing interface message payload sizes. Aggregated bandwidth statistics are exported to `kpi_metrics/bandwidth_stats.json`. These measurements reflect application-layer payload sizes and therefore represent a lower bound on link utilisation under DDS/RTPS transport.

**Delivery rate under impairments.** When impairments are enabled, effective delivery rate is derived by combining publisher-side send counters with receiver-side observed counters (and optionally ACKs for central factor batches). Results are exported to `kpi_metrics/robustness_metrics.json`.

# 6

# Evaluation

This chapter evaluates the collaborative SLAM backends defined in Chapter 4 and realised in Chapter 5. Following the experimental design space $\mathcal{D} = \mathcal{A} \times \mathcal{N} \times \mathcal{Q} \times \mathcal{I}$ introduced in Section 4.1, the evaluation varies (i) backend architecture $\mathcal{A}$ (centralised vs. decentralised), (ii) team size $\mathcal{N}$ (r3–r5), (iii) ROS 2 QoS policy $\mathcal{Q}$, and (iv) injected network impairments $\mathcal{I}$. All runs are analysed with the KPI pipeline described in Section 5.7, producing accuracy, timing, communication, and resource metrics consistent with Section 4.5.

**Research-question coverage.** The chapter is organised to explicitly answer the research questions stated in Chapter 1. Research Question 1 (latency and convergence) is addressed through architecture-specific timing indicators and a shared stabilisation proxy (Section 6.1.3). Research Question 2 (effect of team size) is addressed through the r3–r5 baseline scalability sweep (Section 6.3.2). Research Question 3 (compute and bandwidth under network constraints) is addressed via traffic, delivery, and resource metrics under QoS and impairments (Sections 6.4 and 6.5). Research Question 4 (robustness) is addressed through impairment behaviour and unsupported configurations (Section 6.6).

# 1 Experimental protocol and reporting conventions

## 1.1 Protocol and design-space instantiation

Each experiment is a deterministic dataset replay (Section 5.1) executed for both backends under identical frontend inputs and identical factor streams. The dataset provides two native networking regimes—*WiFi* and *ProRadio*—which differ in the recorded factor-stream characteristics; these are treated as environmental conditions of the protocol rather than tunable parameters.

The baseline configuration uses the reference ROS 2 QoS profile RV-20 (reliable reliability, volatile durability, history depth 20) and applies no synthetic network impairment. QoS experiments modify only $\mathcal{Q}$ while keeping the dataset regime unchanged, and impairment experiments modify only $\mathcal{I}$ using the impairment mechanism described in Section 5.6. For fairness, comparisons are organised around matched tuples $(\mathcal{A}, \mathcal{N}, \text{regime})$ and then one factor is changed at a time. Concretely, the evaluation proceeds as follows: (i) an "apples-to-apples" baseline comparison at r3 under each regime, contrasting the two backends with identical RV-20 QoS and without impairments; (ii) a scalability sweep by repeating the baseline at r4 and r5; (iii) a QoS sensitivity study at r3 (alternate QoS profiles, no impairments); and (iv) an impairment sensitivity study at r3 and r5 (bandwidth caps and blackouts). Unless stated otherwise, the impairment sweep reported in Section 6.5 applies impairments at the factor publishers (uplink/factor-stream degradation), which isolates the effect of constrained constraint availability from backend-internal communication impairments.

Repeat counts depend on the sweep: baseline, QoS, and impairment configurations are repeated five times ($R = 5$). While deterministic replay reduces environmental variance, asynchronous scheduling and ROS 2 buffering can still introduce run-to-run variation in timing and delivery-related KPIs; this is treated explicitly in the aggregation conventions below.

**Result provenance (run outputs).** All numeric results and failure statuses in this chapter are taken from the experiment output folders under `new_eval/out/`: baseline/scalability `baseline_20260204_180031`, QoS `qos_20260205_081932`, and impairments `impair_20260204_191738`.

## 1.2 Reporting conventions

To avoid ambiguity in how results are aggregated, the chapter follows the reporting rules below.

**Repeats.** For each configuration, KPIs are first computed per run and then averaged over repeats ($R$ runs, as specified in Section 6.1.1). Where "[min,max]" ranges are reported, they are computed after averaging the relevant per-robot KPI over repeats.

**Shared convergence proxy $T_{\text{conv}}^{(\text{team})}$.** Where tables present results for both architectures, a shared convergence proxy is reported as $T_{\text{conv}}^{(\text{team})}$ following Section 4.5.1. In tables, this is summarised as mean ± half-width of the 95% CI across repeats. If the stabilisation window is not observed within a run, the value is right-censored at the run end and reported as a lower bound ("≥").

**KPI naming convention.** To avoid confusing architecture-comparable stabilisation metrics with event-semantic proxies, this chapter uses the following naming convention in the discussion: `stable_*` for stabilisation-window metrics (e.g., $T_{\text{conv}}^{(\text{team})}$ and stabilised correction times), `event_*` for event-defined proxies (e.g., time-to-last-broadcast), and `term_*` for termination/stop-condition times (e.g., DDF stop time).

**Statistical treatment (run-level uncertainty).** The experimental unit is a single run (one repeat folder `__rXX`). Unless stated otherwise, uncertainty is summarised across repeats using 95% confidence intervals (CI) computed over run-level KPIs. Where comparisons are naturally matched (e.g., centralised vs. decentralised on the same dataset repeat index, or impairment vs. baseline under the same regime), paired differences are preferred and CIs are computed over the paired run-to-run deltas to reduce sensitivity to shared environmental noise.

**Robot/team aggregation.** Where a KPI is naturally per-robot (e.g., ATE), it is computed per robot and then summarised at team level. In tables, *ATE mean* denotes the team mean across robots. When an *ATE RMSE [min,max]* range is reported, the bracket denotes the minimum and maximum across robots of the repeat-mean per-robot ATE.

**Traffic and delivery.** Traffic (MiB) denotes the total transmitted payload volume aggregated across all participating nodes in the backend under that scenario. For centralised runs, uplink/downlink splits are reported to highlight the broadcast structure. Factor delivery denotes the fraction of expected factor messages received/processed by the backend; *delivery min* reports the worst-case robot (minimum across robots) after averaging over repeats.

**Compute and memory.** CPU mean and RSS mean are taken from the process-monitor signals exported by the KPI pipeline (Section 5.7) and averaged over time and repeats. For centralised runs, these values are dominated by the server-side optimisation process; for decentralised runs they reflect the distributed agent processes.

## 1.3 Timing semantics and convergence definitions

Timing metrics are interpreted with an explicit separation between *dissemination* and *estimate stabilisation*. The centralised backend exposes an unambiguous dissemination event: the server emits global map/pose broadcasts to robots. We

therefore report $t_{\text{global}}$ as a *broadcast/dissemination* proxy (time until the final broadcast observed in the run).

To characterise correction latency in the centralised pipeline, we additionally report loop-closure correction latency (p95), denoted "Corr. p95" in the tables.

Across both backends, "Opt. p95" denotes the p95 of the backend-measured optimisation update duration (compute-only) over all solver updates in a run.

In contrast, the decentralised backend has no single broadcaster and therefore no direct analogue of "last map broadcast". For decentralised runs, "Corr. p95" refers to interface correction stabilisation latency (p95) and acts as a *correction-propagation* proxy. These timing indicators are architecture-specific and must not be compared as if they were the same notion of convergence.

Where a cross-architecture convergence comparison is required, convergence is defined via a shared stabilisation proxy based on receiver-side settling: a per-robot stabilisation time $T_{\text{conv}}^{(r)}$ and a conservative team statistic $T_{\text{conv}}^{(\text{team})} = \max_r T_{\text{conv}}^{(r)}$ (Section 4.5.1). In this chapter, architecture-specific timing indicators are reported alongside accuracy and communication metrics to characterise operational behaviour, while timing-related cross-architecture interpretations are stated conservatively.

# 2 Results overview

The evaluation yields four consistent high-level patterns that guide the detailed discussion in the subsequent sections. First, in the nominal baseline runs, the centralised backend achieves lower ATE than the decentralised backend across both dataset regimes. Second, communication semantics differ structurally: centralised operation is dominated by downlink global broadcasts, whereas decentralised operation is dominated by uplink peer-to-peer interface and factor exchanges. Third, QoS variations have negligible effect on centralised outcomes in the evaluated settings, but modulate decentralised bandwidth through buffering depth without materially changing accuracy in the nominal regime. Finally, in the uplink-only impairment mode used here, severe bandwidth caps delay when information becomes available to the backend and thereby delay centralised dissemination (increasing $t_{\text{global}}$ with essentially constant traffic), while blackouts reduce factor delivery and can trigger instability or failure in some decentralised configurations.

# 3 Baseline comparison under native dataset networking

The baseline establishes a reference operating point for both architectures under the two dataset-native networking regimes, using identical frontend outputs and the same RV-20 QoS profile. Beyond serving as the main architecture comparison, the baseline anchors the subsequent sensitivity studies (QoS and impairments) by providing a common reference for each $(\mathcal{N}, \text{regime})$.

## 3.1 Reference r3 baseline: centralised vs. decentralised

Table 6.1 summarises the r3 baseline. Across both networking regimes, the centralised backend achieves lower trajectory error than the decentralised backend. Under WiFi, the centralised ATE is 2.27 m (range 2.23–2.30 m), compared to 3.58 m (2.77–4.68 m) for the decentralised backend. Under ProRadio, the same pattern holds: 2.16 m (2.12–2.24 m) vs. 3.82 m (2.89–5.51 m).

The timing metrics reflect the different event semantics of the two architectures. For the centralised backend, $t_{\text{global}}$ is a dissemination proxy (time until the last global map broadcast), and Corr. p95 reports loop-closure correction latency (p95). For the decentralised backend, Corr. p95 reports interface correction stabilisation latency (p95) as a correction-propagation proxy. These are reported side-by-side to characterise each pipeline; any strict convergence comparison should be grounded in the shared proxy $T_{\text{conv}}^{(\text{team})}$ (Section 6.1.3).

The baseline exposes the dominant communication patterns. In the centralised WiFi run, downlink map broadcast accounts for 89.8% of the total traffic (49.4 MiB of 55.0 MiB), whereas the decentralised backend transmits almost exclusively uplink interface and factor updates. Under ProRadio, the same qualitative picture remains, with map broadcast constituting 86.5% of the centralised traffic. These structural differences explain why the decentralised backend is more bandwidth-efficient on WiFi at r3 (28.7 MiB vs. 55.0 MiB total), but not necessarily on ProRadio (32.2 MiB vs. 30.3 MiB total, albeit in different directions).

Compute and resource usage align with the architectural split. The centralised backend concentrates computation on the server node (single dominant process), whereas the decentralised backend distributes the optimisation effort across agents (multiple processes). Per-process CPU utilisation is comparable in magnitude, but the decentralised backend incurs a higher *total* CPU demand when summing across agents, and a higher aggregate memory footprint when considering all agent processes. Consistent with the solver structure described in Section 5.4 and Section 5.5, the decentralised optimisation step is shorter (lower p95 optimisation duration) but requires additional time for interface-level corrections to propagate and stabilise. To express efficiency in a normalised way, the evaluation also reports *CPU-seconds per optimisation step*: the time-integral of process CPU utilisation (CPU% over time) divided by the number of solver optimisation steps in the run.

## 3.2 Scalability trend (r3–r5)

Scalability is assessed by repeating the baseline protocol at r4 and r5. Table 6.3 reports the resulting trends. For the decentralised backend, Figure 6.6 visualises how final accuracy relates to DDF termination time as team size increases, and Table 6.2 provides diagnostic counts of inter-robot loop-closure constraints and interface update activity per team size.

For the centralised backend, total traffic grows with team size primarily because the global map broadcast must serve more robots and the map itself

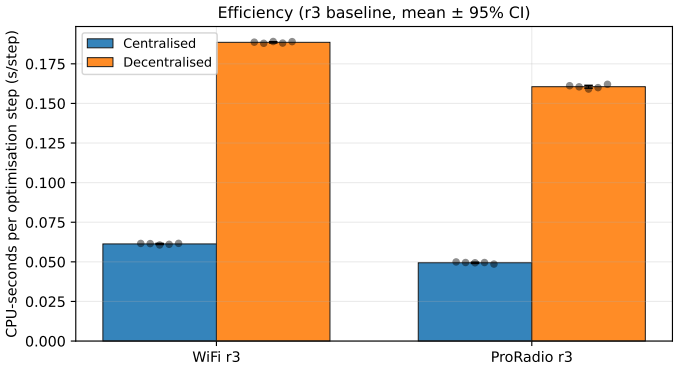


Figure 6.1: Efficiency-normalised metric for the r3 baseline: CPU-seconds per optimisation step. Bars show mean over repeats ($R = 5$); error bars denote 95% CI across repeats, with individual repeats overlaid. Lower values indicate less compute time spent per solver update.

Table 6.1: Baseline comparison for the reference team size (r3) under the dataset-native networking regimes. $t_{\text{global}}$ is a centralised dissemination proxy (time until last global map broadcast). "Corr. p95" is a correction-latency indicator: for centralised runs it reports loop-closure correction latency (p95), while for decentralised runs it reports interface correction stabilisation latency (p95). These timing indicators are architecture-specific; strict cross-architecture convergence comparisons should use the shared stabilisation proxy $T_{\text{conv}}^{(\text{team})}$ (Section 6.1.3).

| Link | Backend | ATE RMSE(m) | $t_{\text{global}}$ (s) | Corr. p95 (s) | $T_{\text{conv}}^{(\text{team})}$ (s) | Opt. p95 (s) | Traffic (MiB) |
|---|---|---|---|---|---|---|---|
| PrRa | Centralised | 2.164 ± 0.000 | 11.5 | 0.096 | 0.01 ± 0.00 | 0.030 | 30.3 (up 4.1 / down |
| PrRa | Decentralised | 3.821 ± 0.072 | – | 14.37 | $\geq 21.33 \pm 5.94$ | 0.020 | 32.2 (up 32.2 / down |
| WiFi | Centralised | 2.270 ± 0.002 | 16.4 | 0.126 | 0.12 ± 0.00 | 0.043 | 55.0 (up 5.6 / down |
| WiFi | Decentralised | 3.581 ± 0.035 | – | 4.79 | 15.19 ± 3.53 | 0.026 | 28.7 (up 28.7 / down |

grows as more trajectories contribute constraints. This is most visible under WiFi, where traffic increases from 55.0 MiB (r3) to 69.0 MiB (r4) and 91.0 MiB (r5). Under ProRadio, the same monotonic growth is observed (30.3 MiB to 74.4 MiB to 86.8 MiB), and $t_{\text{global}}$ increases accordingly, reflecting a longer tail of late map broadcasts.

For the decentralised backend, scalability is driven by peer-to-peer interface exchange frequency and the size of shared summaries. On WiFi, decentralised traffic grows from 28.7 MiB (r3) to 41.4 MiB (r4) and 66.9 MiB (r5), and accuracy degrades at r5 (ATE RMSE 6.66 m with a maximum of 17.04 m), suggesting that interface coordination becomes a limiting factor for maintaining global consistency at this team size under the given dataset regime.

Under ProRadio, decentralised performance is comparatively stable across team sizes: ATE RMSE is 3.82 m (r3), 2.72 m (r4), and 2.90 m (r5), while

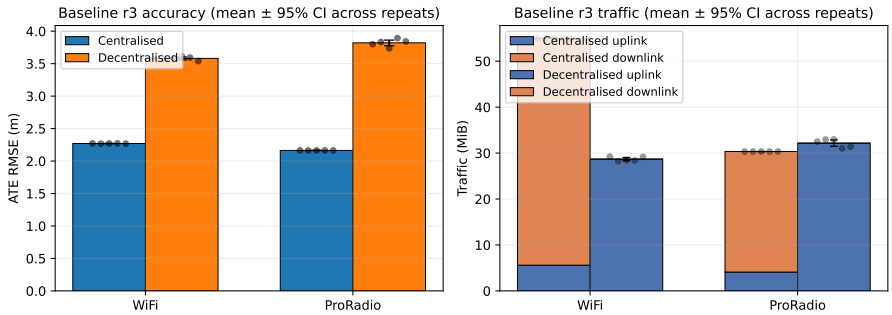


Figure 6.2: Compact summary of the r3 baseline (Table 6.1): ATE RMSE and total traffic with uplink/downlink split. Bars show mean over repeats ($R = 5$); error bars denote 95% CI across repeats.

Table 6.2: Decentralised diagnostic counts in the baseline sweep: number of inter-robot loop-closure constraints (Between factors whose endpoint keys belong to different robot symbols) and number of interface correction updates (count of stabilised interface-correction events). Values are mean ± 95% CI over repeats ($R = 5$).

| Link | Team | Inter-robot loop closures (count) | Interface updates (count) |
|---|---|---|---|
| WiFi | r3 | 390 | 19510 ± 1870 |
| WiFi | r4 | 609 | 26231 ± 3223 |
| WiFi | r5 | 843 | 34644 ± 2990 |
| ProRadio | r3 | 407 | 22858 ± 5315 |
| ProRadio | r4 | 480 | 24055 ± 2408 |
| ProRadio | r5 | 568 | 25570 ± 5564 |

traffic grows from 32.2 MiB to 36.1 MiB and 47.4 MiB. This indicates that, for the evaluated ProRadio sequences, increased team size primarily increases interface-traffic volume without inducing the same r5 accuracy collapse observed under WiFi. Figure 6.5 complements this trend view by showing the per-repeat ATE–traffic dispersion and the resulting trade-off frontier.

# 4 Sensitivity to ROS 2 QoS policy

The QoS study isolates factor $\mathcal{Q}$ by changing only the ROS 2 communication profile while keeping the dataset regime and all other parameters fixed. Two alternate profiles are evaluated: BT-TL-10 and BT-TL-50, which use best-effort reliability and transient-local durability with history depth 10 and 50, respectively (artifact labels: `best_effort_tl_d10` and `best_effort_tl_d50` in the run output folders). This tests whether relaxing delivery guarantees (best-effort) and modifying buffering (depth) alter dissemination/correction timing,

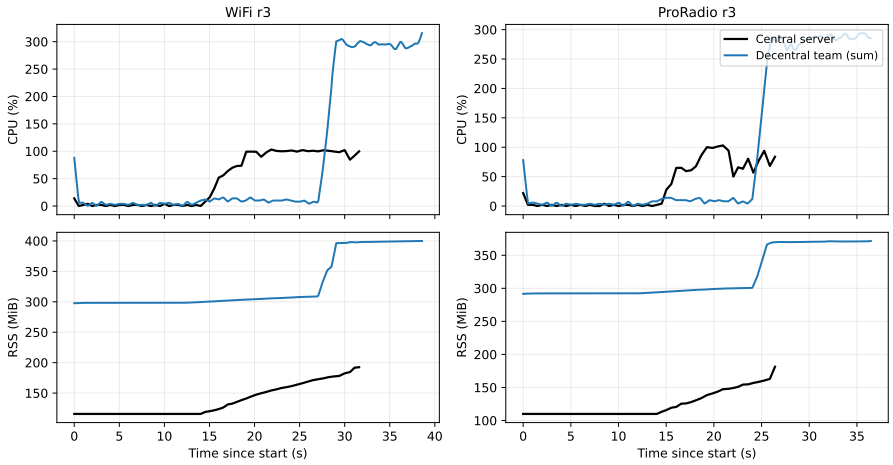


Figure 6.3: Resource traces over time for the r3 baseline: centralised CPU/RSS of the server process vs. decentralised CPU/RSS aggregated across agents (sum over per-agent processes). Time is aligned to the start of each run. These traces support diagnosis of stability issues (e.g., monotonic RSS growth preceding agent crashes) and complement the aggregate means reported in Table 6.1.

bandwidth, or estimation quality.

Table 6.4 shows the r3 results. For the centralised backend, QoS changes are negligible: ATE and traffic remain unchanged within rounding and $t_{\text{global}}$ remains close to the baseline values. In this implementation, the centralised pipeline is dominated by server-side optimisation cadence and periodic broadcast behaviour, and the evaluated QoS variations do not materially change the produced byte volume nor the server broadcast schedule under deterministic replay. Because $t_{\text{global}}$ is defined as the time until the *last* map broadcast, it remains a dissemination-tail indicator rather than a strict convergence instant. Consequently, centralised QoS sensitivity is primarily assessed through accuracy and traffic, while timing-related cross-architecture comparisons are grounded in the shared stabilisation proxy $T_{\text{conv}}^{(\text{team})}$ (Section 6.1.3).

For the decentralised backend, QoS mainly influences bandwidth through history depth. On WiFi r3, BT-TL-50 increases total traffic by about 35.5% relative to BT-TL-10 (33.6 MiB vs. 24.8 MiB). Despite this shift in communication volume, the ATE change remains small (within about 0.02 m), suggesting that the evaluated QoS settings affect buffering overhead more than estimation quality in the nominal regime for the successful WiFi r3 runs.

One decentralised QoS configuration (ProRadio r3 under BT-TL-10) does not complete successfully due to an agent crash (Table 6.7). This point is treated as an unsupported configuration in the current implementation and bounds conclusions about QoS sensitivity under that regime/profile pair.
Figure 6.7 provides a compact visual summary of these QoS shifts in accuracy

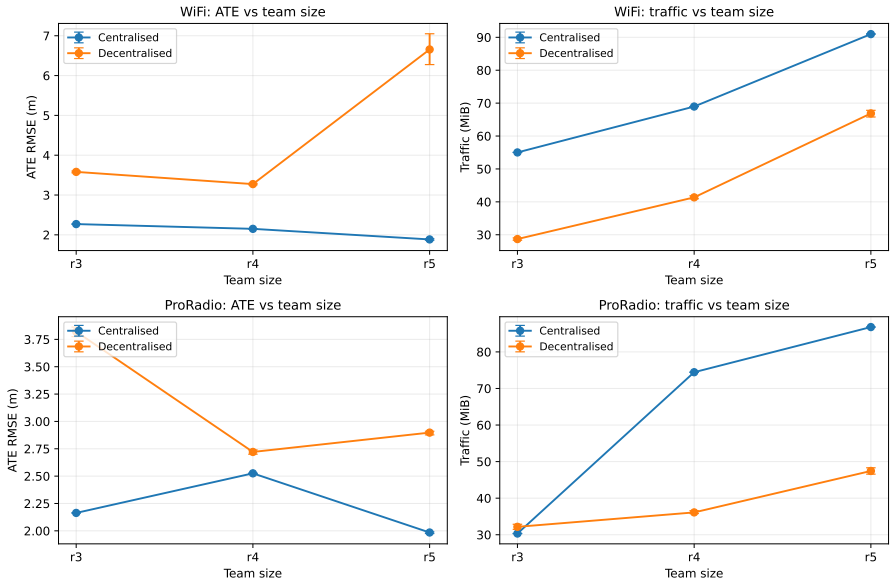


Figure 6.4: Scalability trend in the baseline sweep (Table 6.3): ATE RMSE and traffic vs. team size (r3–r5) for WiFi and ProRadio. Lines show mean over repeats ($R = 5$); error bars denote 95% CI across repeats. Failed runs are marked.

and bandwidth relative to baseline.

# 5 Sensitivity to synthetic network impairments

The impairment study varies factor $\mathcal{I}$ by injecting controlled network degradations on top of the dataset-native regime, using the impairment configuration mechanism described in Section 5.6. In the current sweep, impairments are applied only to the **factor publishing agents** and therefore model **uplink/factor-stream degradation** (constrained factor throughput and temporary robot-side outages), rather than a symmetric impairment of all backend-internal communication. Two impairment families are considered: bandwidth caps (0.25–3.0 Mbps; artifact labels such as `bwcap_0p25mbps`) and periodic blackouts (`blackout_2x`). The objective is to determine how each backend degrades under constrained factor throughput and intermittent factor availability, and whether the dominant failure mode is delayed dissemination/correction propagation, reduced message delivery, or estimator instability.

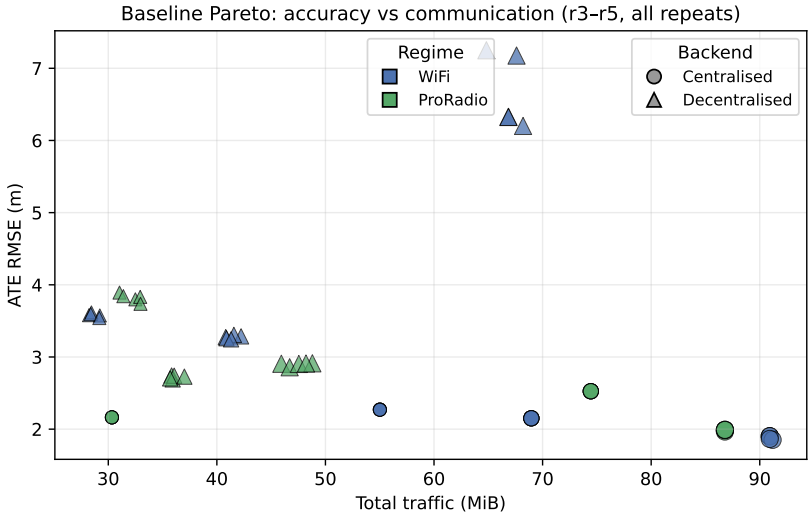


Figure 6.5: Pareto view of baseline trade-offs across team sizes (r3–r5): ATE RMSE vs. total traffic for each successful repeat. This visualisation complements Figure 6.4 by showing per-run dispersion and the accuracy–bandwidth frontier for each architecture.

## 5.1 Centralised backend under impairments

For the centralised backend, bandwidth caps on the factor stream have an intuitive effect: they do not change the total information volume (bytes transmitted remains essentially constant), but they delay when batches arrive at the server and therefore extend the map-broadcast tail. With the most restrictive cap (0.25 Mbps), $t_{\text{global}}$ increases by factors of 9.6× (WiFi r3) and 10.3× (ProRadio r3), and by 8.0× (WiFi r5) and 8.1× (ProRadio r5). In contrast, caps of 1–3 Mbps are nearly indistinguishable from baseline in both timing and accuracy for the evaluated datasets.

Blackout impairments primarily affect delivery rather than throughput. In the centralised pipeline, publisher-side blackouts reduce factor-stream delivery rates and can change estimation error when critical constraints are missed or delayed (e.g., WiFi r3 shows an ATE increase), but runs can still complete because the optimiser continues to operate on the received subset of factors and periodically broadcasts the map.

## 5.2 Decentralised backend under impairments

For the decentralised backend, impairment response is more regime-dependent. Because the current sweep impairs only factor publication, the peer-to-peer interface exchange is *not* directly impaired; instead, bandwidth caps and blackouts change the *availability and timing of new constraints* at each agent. Under WiFi,

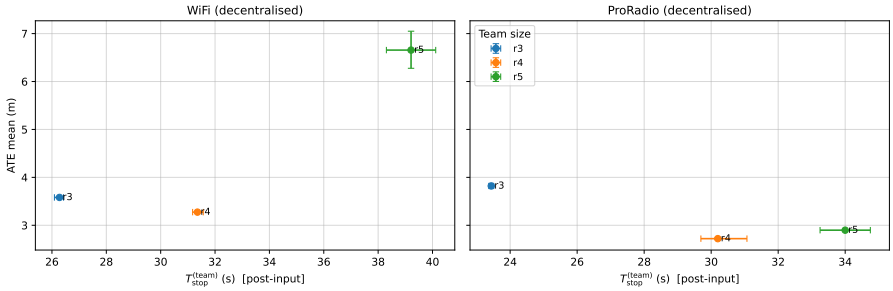


Figure 6.6: Decentralised diagnostic for RQ2: ATE mean vs. DDF termination time. The x-axis reports $T_{\text{stop}}^{(\text{team})}$ (time from `input_end` until all agents emit `ddf_stop`, team statistic = max over robots). Error bars denote 95% CI over repeats ($R = 5$).

the evaluated blackout condition leads to agent failures (Table 6.7), while bandwidth caps produce only modest changes in ATE and traffic for the successful runs. Under ProRadio, the strict 0.25 Mbps cap increases interface correction stabilisation latency (p95) and increases ATE at r3, indicating sensitivity to delayed constraint ingestion and slower correction settling under reduced factor throughput. Blackouts are survivable at r3 but still trigger agent failures at r4 and r5.

# 6 Robustness and unsupported configurations

Table 6.7 lists runs that did not complete successfully and were excluded from quantitative comparisons. These outcomes are treated as *unsupported configurations* in the current implementation, and they bound the generality of scalability, QoS, and impairment conclusions for the affected scenarios.

The dominant failure mode is an agent crash in the decentralised backend under intermittent or delayed delivery, observed in one QoS configuration (ProRadio r3 under BT-TL-10) and under multiple impairment conditions (notably blackout cases across WiFi and ProRadio, and one WiFi r3 bandwidth-cap configuration). Centralised runs complete across all evaluated scenarios, including blackouts, albeit with reduced delivery and, in some cases, increased ATE. Figure 6.9 summarises this support status across the full design space.

## 6.1 Failure mode analysis (decentralised crashes)

Across the failed decentralised runs in Table 6.7, the observed crash signature is consistent: an out-of-range index in GTSAM iSAM2 factor removal (e.g., `IndexError: vector::_M_range_check ... removeFactorIndices ...`). The stack traces in the exported artefacts (`kpi_metrics/agent_error_<rid>.txt`) indicate that the exception is raised in `c_slam_common/isam2.py` during `isam.update(...,`

Table 6.3: Baseline scalability trend across team sizes (r3–r5). Backend: C=centralised, D=decentralised. "Time" denotes $t_{\text{global}}$ for centralised runs (dissemination proxy) and Corr. p95 for decentralised runs (correction-propagation proxy). The shared convergence proxy $T_{\text{conv}}^{(\text{team})}$ is reported as the comparison anchor (mean ± 95% CI across repeats; "≥" indicates right-censoring when stabilisation is not observed). Rows marked `fail` were excluded from trend interpretation.

| Link | Team | B/E | Status | ATE RMSE (m) | Time (s) | $T_{\text{conv}}^{(\text{team})}$ (s) | Opt. p95 (s) | Traffic (MiB) | CPU m |
|---|---|---|---|---|---|---|---|---|---|
| ProRadio | r3 | C | ok | 2.164 ± 0.000 | 11.5 | 0.01 ± 0.00 | 0.030 | 30.3 | 32 |
| ProRadio | r4 | C | ok | 2.526 ± 0.000 | 21.6 | 0.12 ± 0.01 | 0.055 | 74.4 | 52 |
| ProRadio | r5 | C | ok | 1.985 ± 0.013 | 25.0 | 0.17 ± 0.00 | 0.058 | 86.8 | 55 |
| ProRadio | r3 | D | ok | 3.821 ± 0.072 | 14.4 | $\geq 21.33 \pm 5.94$ | 0.020 | 32.2 | 37 |
| ProRadio | r4 | D | ok | 2.721 ± 0.030 | 8.3 | 12.58 ± 1.20 | 0.026 | 36.1 | 35 |
| ProRadio | r5 | D | ok | 2.898 ± 0.028 | 6.0 | $\geq 20.34 \pm 10.35$ | 0.026 | 47.4 | 30 |
| WiFi | r3 | C | ok | 2.270 ± 0.002 | 16.4 | 0.12 ± 0.00 | 0.043 | 55.0 | 45 |
| WiFi | r4 | C | ok | 2.151 ± 0.000 | 20.6 | 0.13 ± 0.00 | 0.059 | 69.0 | 51 |
| WiFi | r5 | C | ok | 1.885 ± 0.031 | 26.3 | 0.15 ± 0.01 | 0.062 | 91.0 | 57 |
| WiFi | r3 | D | ok | 3.581 ± 0.035 | 4.8 | 15.19 ± 3.53 | 0.026 | 28.7 | 38 |
| WiFi | r4 | D | ok | 3.274 ± 0.030 | 4.9 | 11.53 ± 0.45 | 0.026 | 41.4 | 35 |
| WiFi | r5 | D | ok | 6.656 ± 0.635 | 6.2 | 23.85 ± 1.55 | 0.028 | 66.9 | 33 |

`removeFactorIndices=...)` and is triggered from the decentralised agent update loop (`c_slam_decentral/agents.py` via `c_slam_decentral/mp_runner.py`). This points to an implementation-level bug: the removal index list becomes inconsistent with the internal factor container size.

While the immediate failure is not an out-of-memory event, the resource traces provide supporting context for why these crashes are more likely under constrained conditions. In representative impairment failures, one or more agents exhibit monotonic RSS growth and high CPU bursts during prolonged intermittency (e.g., in a WiFi r5 blackout run, an agent's RSS grows by ≈54 MiB over the run), suggesting queue/backlog accumulation and delayed processing. These conditions can plausibly increase the likelihood of stale or invalid factor-removal indices (e.g., due to out-of-order updates or mismatched bookkeeping across rounds). For evaluation, these points are treated conservatively as unsupported configurations; robustness conclusions for decentralised operation under intermittency therefore remain conditional on resolving this stability issue.

# 7 Synthesis and limitations

This section synthesises the results by explicitly answering the research questions from Chapter 1, and highlights the main limitations that remain.

Table 6.4: QoS sensitivity at r3. Two alternate profiles are evaluated: BT-TL-10 and BT-TL-50, which use best-effort reliability and transient-local durability with history depth 10 and 50, respectively. Baseline (RV-20) results are reported in Table 6.1. "Time" denotes $t_{\text{global}}$ for centralised runs and Corr. p95 for decentralised runs. $T_{\text{conv}}^{(\text{team})}$ is the shared stabilisation proxy (mean ± 95% CI; "≥" indicates right-censoring). Rows marked `fail` indicate at least one repeat crashed.

| Link | B/E | QoS profile | Status | ATE mean (m) | Traffic (MiB) | Time (s) | $T_{\text{conv}}^{(\text{team})}$ (s) |
|---|---|---|---|---|---|---|---|
| WiFi | C | BT-TL-10 | ok | 2.272 ± 0.000 | 55.0 | 16.4 | 0.12 ± 0.00 |
| WiFi | C | BT-TL-50 | ok | 2.272 ± 0.000 | 55.0 | 16.4 | 0.12 ± 0.00 |
| WiFi | D | BT-TL-10 | ok | 3.598 ± 0.032 | 24.8 | 7.0 | 17.12 ± 1.45 |
| WiFi | D | BT-TL-50 | ok | 3.578 ± 0.030 | 33.6 | 4.4 | 13.49 ± 1.08 |
| ProRadio | C | BT-TL-10 | ok | 2.164 ± 0.000 | 30.3 | 11.7 | 0.01 ± 0.00 |
| ProRadio | C | BT-TL-50 | ok | 2.164 ± 0.000 | 30.3 | 11.7 | 0.01 ± 0.00 |
| ProRadio | D | BT-TL-10 | fail | – | – | – | – |
| ProRadio | D | BT-TL-50 | ok | 3.859 ± 0.038 | 37.2 | 12.7 | $\geq 24.54 \pm 1.09$ |

**RQ1: How do architectures differ in global map update latency and convergence time?** In the baseline, centralised operation provides a clear dissemination event, with $t_{\text{global}}$ of 11.5 s (ProRadio r3) and 16.4 s (WiFi r3) (Table 6.1). Decentralised operation has no analogue of a "last broadcast"; instead, correction propagation is captured by Corr. p95, which is 14.4 s (ProRadio r3) and 4.8 s (WiFi r3). These indicators quantify different pipeline stages and are not directly comparable. When the discussion requires a shared notion of convergence, the appropriate reference is the stabilisation proxy $T_{\text{conv}}^{(\text{team})}$ defined in Section 6.1.3.

**RQ2: What is the impact on latency as the number of collaborating agents increases?** For the centralised backend, increasing team size increases both traffic and the dissemination tail: $t_{\text{global}}$ rises from 11.5 s (ProRadio r3) to 25.0 s (ProRadio r5), and from 16.4 s (WiFi r3) to 26.3 s (WiFi r5) (Table 6.3). For the decentralised backend, Corr. p95 does not increase monotonically with team size in these datasets and regimes; instead it shows regime-dependent behaviour (e.g., ProRadio r3: 14.4 s, r4: 8.3 s, r5: 6.0 s; WiFi r3: 4.8 s, r4: 4.9 s, r5: 6.2 s). This suggests that decentralised latency is dominated by interface-level correction dynamics and scheduling effects rather than by a simple "more robots implies more latency" rule.

**RQ3: What are the computational loads and communication bandwidth requirements under varying network constraints?** Under nominal conditions, centralised communication is dominated by downlink broadcast (e.g., 49.4 MiB downlink of 55.0 MiB total on WiFi r3), whereas decentralised traffic is almost entirely uplink (e.g., 28.7 MiB uplink on WiFi r3) (Table 6.1). QoS

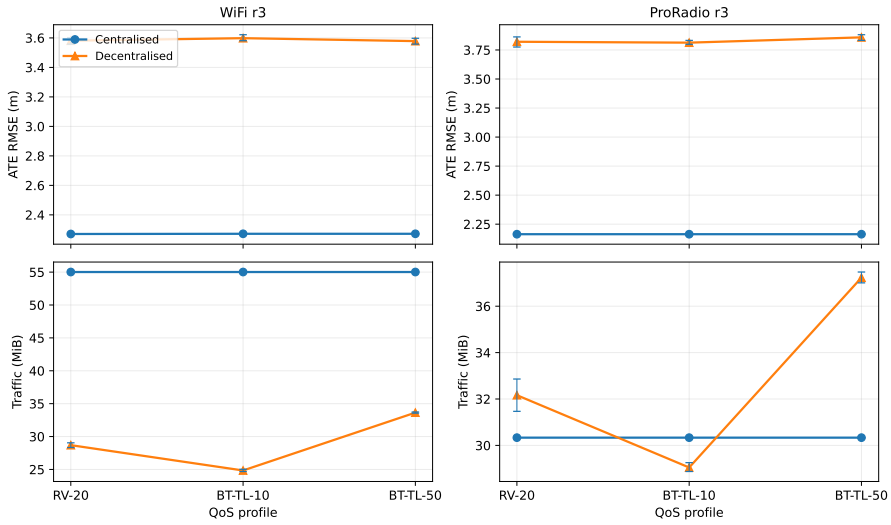


Figure 6.7: QoS sensitivity (r3): slope-chart style summary of how ATE and traffic shift from the baseline profile (RV-20) under BT-TL-10 and BT-TL-50. Lines show mean over repeats ($R = 5$); error bars denote 95% CI across repeats. Failed configurations are marked.

changes do not measurably affect the centralised pipeline at r3, but they modulate decentralised bandwidth through buffering depth (Table 6.4). Under severe bandwidth caps (0.25 Mbps), centralised runs retain essentially constant traffic but exhibit strongly delayed dissemination ($t_{\text{global}}$ increases by roughly 8–10×), whereas decentralised ProRadio r3 exhibits increased correction latency and degraded ATE (Table 6.6). Together, these results indicate that centralised operation is mainly sensitive to uplink throughput in terms of *when* information can be disseminated (timing), while decentralised operation is sensitive to throughput in terms of *whether and how quickly* interface consistency can be restored (timing and accuracy), and in some blackout cases, whether it remains stable at all. *Note.* Because the impairment sweep presented here is publisher-impaired (uplink-only), these "network constraints" should be interpreted as constraints on factor-stream availability. A complementary solver-impaired sweep would be required to directly quantify sensitivity to impairments on decentralised peer-to-peer exchange and on centralised downlink dissemination.

**RQ4: How does the choice of architecture affect robustness to common real-world challenges?** Under blackouts, centralised runs complete with reduced delivery and, in some scenarios, increased ATE (Table 6.5). In contrast, decentralised operation exhibits agent failures under several blackout configurations (notably WiFi r3/r5 and ProRadio r4/r5) (Table 6.7). These failures indicate that robustness conclusions for decentralised operation under

Table 6.5: Impact of representative network impairments on the centralised backend. Bandwidth caps of 1–3 Mbps were near-identical to baseline and are omitted here; only the most restrictive cap (0.25 Mbps) is shown.

| Scenario | Impairment | $t_{\text{global}}$ (s) | ATE mean (m) | Factor delivery min | Traffic (MiB) |
|---|---|---|---|---|---|
| WiFi r3 | none | 16.4 | 2.270 ± 0.002 | 1.000 | 55.0 |
| WiFi r3 | bwcap 0.25 Mbps | 158.1 | 2.272 ± 0.000 | 1.000 | 55.0 |
| WiFi r3 | blackout 2x | 10.2 | 3.192 ± 0.243 | 0.499 | 24.3 |
| WiFi r5 | none | 26.3 | 1.885 ± 0.031 | 1.000 | 91.0 |
| WiFi r5 | bwcap 0.25 Mbps | 210.6 | 1.902 ± 0.000 | 1.000 | 90.9 |
| WiFi r5 | blackout 2x | 7.9 | 1.765 ± 0.058 | 0.263 | 22.8 |
| ProRadio r3 | none | 11.5 | 2.164 ± 0.000 | 1.000 | 30.3 |
| ProRadio r3 | bwcap 0.25 Mbps | 118.4 | 2.164 ± 0.000 | 1.000 | 30.3 |
| ProRadio r3 | blackout 2x | 11.7 | 1.722 ± 0.093 | 0.742 | 26.9 |
| ProRadio r5 | none | 25.0 | 1.985 ± 0.013 | 1.000 | 86.8 |
| ProRadio r5 | bwcap 0.25 Mbps | 202.0 | 1.990 ± 0.000 | 1.000 | 86.8 |
| ProRadio r5 | blackout 2x | 21.2 | 1.652 ± 0.028 | 0.400 | 74.1 |

intermittent connectivity are conditional on the stability/supportability of the current implementation. Treating these points as unsupported is conservative, but it also highlights a concrete engineering requirement for decentralised deployment: robustness mechanisms must include not only estimator-level resilience to missing factors, but also software-level stability under prolonged queueing, delayed delivery, or intermittent connectivity. *Note.* In this implementation, blackouts are applied at factor publication time and therefore primarily model temporary loss of a robot's outgoing constraint stream. They do not directly impair peer-to-peer interface exchange unless the solver-side injection mode is enabled; robustness interpretations are scoped accordingly.

**Limitations and practical implications.** Two limitations are most relevant for interpreting the results. First, while repeats were increased to $R = 5$, asynchronous scheduling and ROS 2 buffering can still introduce dispersion and non-Gaussian timing variability; this is addressed by reporting run-level CIs, but additional repeats for a small subset of key configurations would further strengthen quantitative claims. Second, several decentralised configurations remain unsupported due to agent crashes (notably WiFi r4 under QoS variants and multiple blackout impairment conditions), which bounds conclusions about intermediate team-size behaviour and about robustness under severe intermittency. For the final submission, these points should either be complemented by a focused failure analysis (logs, memory growth, deadlock conditions) or clearly stated as implementation limitations of the evaluated decentralised backend.

**Note on RPE.** Relative pose error (RPE) is defined in Section 4.5 as a drift-oriented metric; this chapter focuses on ATE to keep tables compact. RPE values are available in the KPI exports and can be reported in an appendix if

Table 6.6: Impact of representative network impairments on the decentralised backend (DDF-style). "Iface p95" is interface correction stabilisation latency (p95). Rows marked `fail` indicate runs where at least one agent crashed.

| Scenario | Impairment | Status | ATE mean (m) | Iface p95 (s) | Factor delivery min | Traffic (MiB) |
|---|---|---|---|---|---|---|
| WiFi r3 | none | ok | 3.581 ± 0.035 | 4.8 | 0.995 | 28.7 |
| WiFi r3 | bwcap 0.25 Mbps | ok | 3.465 ± 0.024 | 9.5 | 0.989 | 28.0 |
| WiFi r3 | blackout 2x | fail | – | – | – | – |
| WiFi r5 | none | ok | 6.656 ± 0.635 | 6.2 | 0.998 | 66.9 |
| WiFi r5 | bwcap 0.25 Mbps | ok | 7.603 ± 0.000 | 1.6 | 0.944 | 64.2 |
| WiFi r5 | blackout 2x | fail | – | – | – | – |
| ProRadio r3 | none | ok | 3.821 ± 0.072 | 14.4 | 1.000 | 32.2 |
| ProRadio r3 | bwcap 0.25 Mbps | ok | 4.297 ± 0.044 | 22.7 | 0.990 | 28.9 |
| ProRadio r3 | blackout 2x | ok | 2.768 ± 0.031 | 10.3 | 0.722 | 29.7 |
| ProRadio r5 | none | ok | 2.898 ± 0.028 | 6.0 | 1.000 | 47.4 |
| ProRadio r5 | bwcap 0.25 Mbps | ok | 4.876 ± 0.000 | 1.4 | 0.980 | 41.8 |
| ProRadio r5 | blackout 2x | fail | – | – | – | – |

Table 6.7: Runs that did not complete successfully and were excluded from quantitative comparisons.

| Scenario | Study | B/E | Condition | Failure mode |
|---|---|---|---|---|
| proradio-r3-proradio | qos | D | best_effort_tl_d10 | agent c crashed |
| proradio-r4-proradio | impair | D | blackout_2x | agent d crashed |
| proradio-r5-proradio | impair | D | blackout_2x | agent e crashed |
| wifi-r3-wifi | impair | D | blackout_2x | agent c crashed |
| wifi-r3-wifi | impair | D | bwcap_3p0mbps | agent c crashed |
| wifi-r4-wifi | impair | D | bwcap_0p25mbps | agent b crashed |
| wifi-r4-wifi | impair | D | blackout_2x | agent d crashed (and b in one repeat) |
| wifi-r5-wifi | impair | D | blackout_2x | agent e crashed |

required by the final write-up.

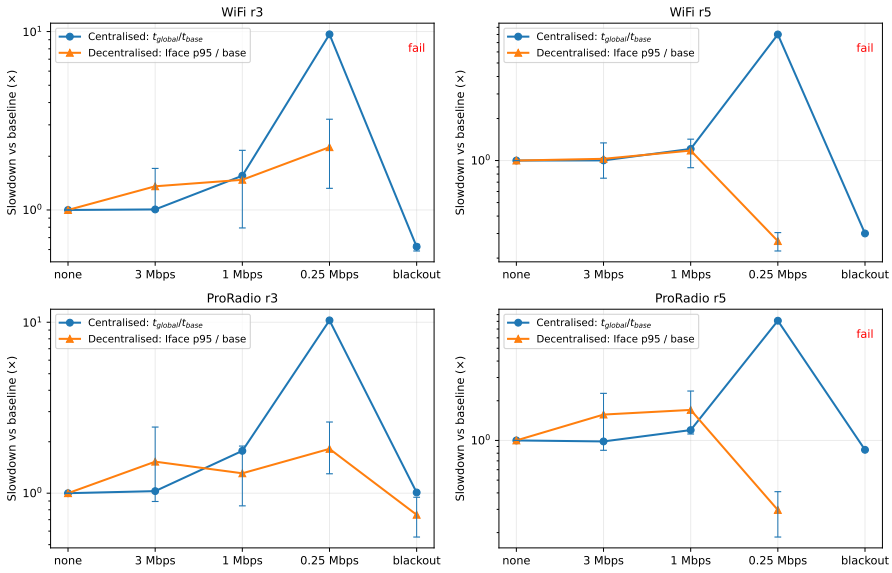


Figure 6.8: Normalised impairment sensitivity (slowdown vs. baseline) under uplink-only (publisher-impaired) degradations (Tables 6.5 and 6.6): centralised $t_{\text{global}}/t_{\text{base}}$ and decentralised Iface p95/base across bandwidth caps and blackouts. Points show mean over repeats ($R = 5$); error bars denote 95% CI across repeats. Failed runs are marked.


Figure 6.9: Robustness matrix summarising which configurations are supported (all repeats ok) vs. unsupported (at least one repeat fails) across the three studies: baseline, QoS, and impairments. This view complements the per-table `fail` annotations by providing a compact support-status overview.

# 7

# Conclusion and Future Works

This research thesis set out to provide a controlled, implementation-grounded comparison of two representative backend paradigms for multi-agent collaborative SLAM. First, it introduces a unified and reproducible ROS 2-based evaluation framework that executes both architectures under a common dataset, factor representation, and KPI instrumentation. This testbed enables fair side-by-side comparisons across latency, accuracy, communication, and resource utilisation. Second, it delivers two concrete backend implementations that represent contrasting architectural choices: a centralised incremental backend that maintains a global factor graph and publishes global updates, and a decentralised DDF-style backend that performs per-agent optimisation and exchanges interface information peer-to-peer. Third, it proposes an impairment-aware experimentation methodology that models packet loss, delay, and bandwidth limitations and applies these consistently across architectures, thereby enabling a systematic assessment of robustness under degraded communication. Finally, the evaluation provides a quantitative characterisation of architectural trade-offs through an empirical analysis spanning baseline operation (3 robots), scalability conditions (4–5 robots), and impaired-network scenarios, reporting ATE/RPE, latency and convergence behaviour, bandwidth consumption, CPU load, and memory footprint.

Taken together, the baseline, scaling, and impairment evaluations provide clear guidance on when each backend is preferable. When global accuracy and predictable convergence dominate system requirements, the centralised backend

is the more suitable choice in the evaluated configurations, particularly as team size grows, where DDF shows both accuracy degradation and the potential for latency inflation due to coordination overhead. When bandwidth is the primary constraint, the decentralised backend is strongly advantageous, consistently achieving large uplink reductions, avoiding downlink entirely, and remaining memory-efficient. Under degraded communication, both systems degrade, but DDF is more sensitive when peer-to-peer corrections are reduced.

Although the presented comparison is intentionally controlled to ensure fairness and interpretability, several limitations remain. The evaluation relies on COSMO-Bench pre-computed factors, which abstracts away frontend-induced effects and therefore does not capture variability introduced by online data association, loop closure discovery dynamics, or keyframe selection policies. In addition, the study contrasts two representative architectural extremes, centralised versus decentralised rather than exploring the broader design spectrum that includes hierarchical, brokered, and opportunistically hybrid systems. The scaling analysis is limited to a maximum of five robots in the reported experiments, and larger teams, heterogeneous compute capabilities, or asymmetric sensing configurations may alter the observed trade-offs. Finally, network impairments are modelled and applied systematically to preserve fairness across architectures; however, real deployments may exhibit more complex dynamics such as mobility-driven link variability, interference, topology changes, and extended partitions that are not fully represented by the impairment models used here.

Building on these findings and limitations, several directions appear promising. One priority is the implementation and evaluation of hybrid and adaptive backends that interpolate between centralised and decentralised operation, for example through temporary brokers, cluster heads, or edge-offload policies that adjust as network conditions change. A second direction is to improve distributed optimisation by investigating interface scheduling, prioritised constraint exchange, and more robust distributed solvers, with the goal of reducing DDF sensitivity to missing peer updates and mitigating coordination overhead at larger team sizes. Third, reintroducing online frontends or comparing multiple frontend variants would enable an end-to-end evaluation of how backend architectural choices interact with real-time loop closure discovery, outlier handling, and sensor heterogeneity. Finally, moving from single-machine multi-process emulation to multi-host deployment across physical machines would provide a more faithful representation of timing, contention, and network effects that arise in realistic multi-robot systems.

# Bibliography


[1] Cesar Cadena, Luca Carlone, Henry Carrillo, Yasir Latif, Davide Scaramuzza, José Neira, Ian Reid, and John J. Leonard. Past, present, and future of simultaneous localization and mapping: Toward the robust-perception age. *IEEE Transactions on Robotics*, 32(6):1309–1332, 2016.

[2] Yun Chang, Kamak Ebadi, Christopher E Denniston, Muhammad Fadhil Ginting, Antoni Rosinol, Andrzej Reinke, Matteo Palieri, Jingnan Shi, Arghya Chatterjee, Benjamin Morrell, et al. Lamp 2.0: A robust multi-robot slam system for operation in challenging large-scale underground environments. *IEEE Robotics and Automation Letters*, 7(4):9175–9182, 2022.

[3] Yun Chang, Yulun Tian, Jonathan P How, and Luca Carlone. Kimera-multi: a system for distributed multi-robot metric-semantic simultaneous localization and mapping. In *2021 IEEE International Conference on Robotics and Automation (ICRA)*, pages 11210–11218. IEEE, 2021.

[4] Weifeng Chen, Xiyang Wang, Shanping Gao, Guangtao Shang, Chengjun Zhou, Zhenxiong Li, Chonghui Xu, and Kai Hu. Overview of multi-robot collaborative slam from the perspective of data fusion. *Machines*, 11(6):653, 2023.

[5] Ying Chen, Hazer Inaltekin, and Maria Gorlatova. Adaptslam: Edge-assisted adaptive slam with resource constraints via uncertainty minimization. In *IEEE INFOCOM 2023-IEEE Conference on computer communications*, pages 1–10. IEEE, 2023.

[6] Titus Cieslewski, Siddharth Choudhary, and Davide Scaramuzza. Data-efficient decentralized visual slam. In *2018 IEEE international conference on robotics and automation (ICRA)*, pages 2466–2473. IEEE, 2018.

[7] Alexander Cunningham, Vadim Indelman, and Frank Dellaert. Ddf-sam 2.0: Consistent distributed smoothing and mapping. In *2013 IEEE international conference on robotics and automation*, pages 5220–5227. IEEE, 2013.

[8] Alexander Cunningham, Manohar Paluri, and Frank Dellaert. Ddf-sam: Fully distributed slam using constrained factor graphs. In *2010 IEEE/RSJ International Conference on Intelligent Robots and Systems*, pages 3025–3030. IEEE, 2010.

[9] Jeffrey Delmerico, Stefano Mintchev, Alessandro Giusti, Boris Gromov, Kamilo Melo, Tomislav Horvat, Cesar Cadena, Marco Hutter, Auke Ijspeert, Dario Floreano, et al. The current state and future outlook of rescue robotics. *Journal of Field Robotics*, 36(7):1171–1191, 2019.

[10] Isaac Deutsch, Ming Liu, and Roland Siegwart. A framework for multi-robot pose graph slam. In *2016 IEEE International Conference on Real-time Computing and Robotics (RCAR)*, pages 567–572, 2016.

[11] Dapeng Feng, Yuhua Qi, Shipeng Zhong, Zhiqiang Chen, Qiming Chen, Hongbo Chen, Jin Wu, and Jun Ma. S3e: A multi-robot multimodal dataset for collaborative slam. *IEEE Robotics and Automation Letters*, 2024.

[12] Giorgio Grisetti, Rainer Kümmerle, Cyrill Stachniss, and Wolfram Burgard. A tutorial on graph-based slam. *IEEE Intelligent Transportation Systems Magazine*, 2(4):31–43, 2010.

[13] Ben Grocholsky, James Keller, Vijay Kumar, and George Pappas. Cooperative air and ground surveillance. *IEEE Robotics & Automation Magazine*, 13(3):16–25, 2006.

[14] Marco Karrer, Patrik Schmuck, and Margarita Chli. Cvi-slam—collaborative visual-inertial slam. *IEEE Robotics and Automation Letters*, 3(4):2762–2769, 2018.

[15] Navroop Kaur and Aanchal Sharma. Robotics and automation in manufacturing processes. In *Intelligent Manufacturing*, pages 97–109. CRC Press, 2025.

[16] Pierre-Yves Lajoie and Giovanni Beltrame. Swarm-slam: Sparse decentralized collaborative simultaneous localization and mapping framework for multi-robot systems. *IEEE Robotics and Automation Letters*, 9(1):475–482, 2023.

[17] Pierre-Yves Lajoie, Benjamin Ramtoula, Yun Chang, Luca Carlone, and Giovanni Beltrame. Door-slam: Distributed, online, and outlier resilient slam for robotic teams. *IEEE Robotics and Automation Letters*, 5(2):1656–1663, 2020.

[18] Pierre-Yves Lajoie, Benjamin Ramtoula, Fang Wu, and Giovanni Beltrame. Towards collaborative simultaneous localization and mapping: a survey of the current research landscape. *Field Robotics*, 2:971–1000, 2022.

[19] Daniel McGann, Easton R Potokar, and Michael Kaess. Cosmo-bench: A benchmark for collaborative slam optimization. *arXiv preprint arXiv:2508.16731*, 2025.

[20] Manthan Patel, Aditya Bandopadhyay, and Aamir Ahmad. Collaborative mapping of archaeological sites using multiple uavs. In *International Conference on Intelligent Autonomous Systems*, pages 54–70. Springer, 2021.

[21] Manthan Patel, Marco Karrer, Philipp Bänninger, and Margarita Chli. Covins-g: A generic back-end for collaborative visual-inertial slam. *arXiv preprint arXiv:2301.07147*, 2023.

[22] L. Riazuelo, Javier Civera, and J.M.M. Montiel. C2tam: A cloud framework for cooperative tracking and mapping. *Robotics and Autonomous Systems*, 62(4):401–413, 2014.

[23] Angela Ribeiro and Jesus Conesa-Muñoz. Multi-robot systems for precision agriculture. In *Innovation in agricultural robotics for precision agriculture: A roadmap for integrating robots in precision agriculture*, pages 151–175. Springer, 2021.

[24] Patrik Schmuck and Margarita Chli. Ccm-slam: Robust and efficient centralized collaborative monocular simultaneous localization and mapping for robotic teams. *Journal of Field Robotics*, 36(4):763–781, 2019.

[25] Patrik Schmuck, Thomas Ziegler, Marco Karrer, Jonathan Perraudin, and Margarita Chli. Covins: Visual-inertial slam for centralized collaboration. In *2021 IEEE International Symposium on Mixed and Augmented Reality Adjunct (ISMAR-Adjunct)*, pages 171–176. IEEE, 2021.

[26] Abdulhamit Sevgi Ostim, Ahmet Murat Kadioğlu Ostim, and Alpaslan Durmuş Ostim. Using of robotic systems in transportation. In *IEEE International Conference on Cognitive Mobility*, pages 458–468. Springer, 2024.

[27] David Silvera-Tawil. Robotics in healthcare: a survey. *SN Computer Science*, 5(1):189, 2024.

[28] Jürgen Sturm, Nikolas Engelhard, Felix Endres, Wolfram Burgard, and Daniel Cremers. A benchmark for the evaluation of rgb-d slam systems. In *2012 IEEE/RSJ international conference on intelligent robots and systems*, pages 573–580. IEEE, 2012.

[29] Hamid Taheri and Zhao Chun Xia. Slam; definition and evolution. *Engineering Applications of Artificial Intelligence*, 97:104032, 2021.

[30] Yulun Tian, Yun Chang, Fernando Herrera Arias, Carlos Nieto-Granda, Jonathan P How, and Luca Carlone. Kimera-multi: Robust, distributed, dense metric-semantic slam for multi-robot systems. *IEEE Transactions on Robotics*, 38(4), 2022.

[31] Hao Xu, Peize Liu, Xinyi Chen, and Shaojie Shen. D 2 slam: Decentralized and distributed collaborative visual–inertial slam system for aerial swarm. *IEEE Transactions on Robotics*, 40:3445–3464, 2024.

[32] Shipeng Zhong, Hongbo Chen, Yuhua Qi, Dapeng Feng, Zhiqiang Chen, Jin Wu, Weisong Wen, and Ming Liu. Colrio: Lidar-ranging-inertial centralized state estimation for robotic swarms. In *2024 IEEE International Conference on Robotics and Automation (ICRA)*, pages 3920–3926. IEEE, 2024.

[33] Shipeng Zhong, Yuhua Qi, Zhiqiang Chen, Jin Wu, Hongbo Chen, and Ming Liu. Dcl-slam: A distributed collaborative lidar slam framework for a robotic swarm. *IEEE sensors journal*, 24(4):4786–4797, 2023.

[34] Fangcheng Zhu, Yunfan Ren, Longji Yin, Fanze Kong, Qingbo Liu, Ruize Xue, Wenyi Liu, Yixi Cai, Guozheng Lu, Haotian Li, et al. Swarm-lio2: Decentralized, efficient lidar-inertial odometry for uav swarms. *IEEE Transactions on Robotics*, 2024.

[35] Danping Zou, Ping Tan, and Wenxian Yu. Collaborative visual slam for multiple agents: A brief survey. *Virtual Reality & Intelligent Hardware*, 1(5):461–482, 2019.

[36] Chenle Zuo, Zhao Feng, and Xiaohui Xiao. Ccmd-slam: Communication-efficient centralized multirobot dense slam with real-time point cloud maintenance. *IEEE Transactions on Instrumentation and Measurement*, 73:1–12, 2024.

# A

# Appendix